The Effect of Subgrid Physics Models on the Pattern Speed of Bars in Cosmological Simulations

BROOK, ALEXANDER,MARK

The Effect of Subgrid Physics Models on the Pattern Speed of Bars in Cosmological Simulations

Alexander Brook

A thesis presented for the degree of
Master of Science

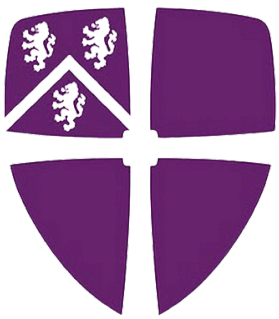

Institute for Computational Cosmology
The University of Durham
United Kingdom

November 2023

The Effect of Subgrid Physics Models on the Pattern Speed of Bars in Cosmological Simulations

Alexander Brook

Abstract

The amount of dark matter in the central region of galaxies is intimately linked to the slowdown of galactic bars. Recent work has revealed a tension between bars that are observed in the local universe and those produced in cosmological hydrodynamical simulations at $z = 0$. Observed bars are found to be 'fast', i.e. to have a small ratio between the corotation radius and bar length, while those in the simulations are 'slow', i.e. the corotation radius much larger than the bar length. Recent work has been carried out in an attempt to find the root cause of this discrepancy, and indeed to explore whether fast bars can exist within a ΛCDM universe. The ratio of stars to dark matter, along with other properties such as gas fraction and velocity dispersion, has been linked to the evolution of bars. The resolution of simulations is often cited as the underlying cause of differences between simulations. In this work, I explore the slowdown of bars in two sets of cosmological zoom-in simulations which are identical, apart from their galaxy formation model (i.e. the subgrid physics). I then study how the slowdown of bars in these two models is related to parameters such as the stellar-to-dark matter ratio, the gas fraction and velocity dispersion, all of which are determined by the subgrid physics itself. Using halos from the Auriga suite of zoom-in cosmological simulations, I rerun them with the subgrid physics model from IllustrisTNG. I find that the bars in Auriga are faster than those run with the TNG model, i.e. Auriga have a smaller ratio of the corotation radius to bar length. The bars in TNG are shorter and stronger than in the Auriga model. In terms of global halo properties, Auriga galaxies have a greater stellar mass in their disc, are more baryon dominated at 30kpc, have a greater gas fraction in the disc. They also have a lower stellar velocity dispersion within a disc of radius 6kpc and height 1kpc from the centre. All of these differences lead to the conclusion that the subgrid physics model has a profound effect on the overall properties of a galaxy, include the speed of the bar. We therefore show that the changes in subgrid physics can have a significant effect on the dynamical properties of barred spiral galaxies and, as such, the dynamical properties of bars can be used to constrain models of galaxy formation and evolution.

Supervisors: Dr Francesca Fragkoudi and Dr Azadeh Fattahi

Contents

Chapter 1

Introduction

1.1 Bars in Observation and Simulation

Galactic bars are elongated rotating structures that exist in a majority of disc galaxies in the local universe (e.g. Eskridge et al. 2000, Menendez-Delmestre et al. 2007, Marinova & Jogee 2007, etc.), as well as our own Milky Way (e.g. Peters 1975, Blitz & Spergel 1991). At low redshift, ($0.01 < z < 0.06$), data from the Galaxy Zoo finds the bar fraction in discs to be 30% (Masters et al. 2011). The observed bar fraction can vary, leading to different conclusions between studies, however it is clear that bars are a common feature of disc galaxies. Bars are also found at high redshifts, with data from the James Webb Space Telescope (JWST) putting the bar fraction at 6.6% in the redshift region $2 \leq z < 3$ (Le Conte et al. 2023). JWST data has also been used to identify the oldest bar yet discovered, at a redshift of $z = 2.312$ (Guo et al. 2023). As bars are extant across cosmic time in a significant proportion of discs, they are a key area of study if we are to gain a deeper understanding of galaxy dynamics and evolution.

Discs that host bars are influenced significantly by them as they drive secular processes and redistribute angular momentum outwards from the inner regions (Lynden-Bell & Kalnajs 1972, Athanassoula 2005). Bars also exert a torque on the gas in the interstellar medium (ISM), inducing shocks funnels gas towards the central kpc (Athanassoula 1992, Yu et al. 2022). There is debate around the impact of this process on star formation rates, with evidence to suggest that bars can enhance star formation within the bar region (Heckman 1980, Ellison et al. 2011, Zee et al. 2023) or suppress it (Khoperskov et al. 2018, Géron et al. 2021). Whether there is a connection between bars and active galactic nuclei (AGN) is another area of debate, with some finding observational evidence to suggest that the bar fraction is greater in galaxies that host AGN (e.g. Alonso et al. 2013, Cisternas

et al. 2015, Silva-Lima et al. 2022). Other studies identify no link between the two (Gadotti & Eustáquio de Souza 2004, Lee et al. 2012).

Recursive structures can also be found in barred galaxies, with the possibility of a second bar forming in the central region of the disc. Secondary bars have been identified in approximately 25% of barred spirals (Erwin & Sparke 2002). It is thought that they contribute to the fueling of AGN through the exchange of angular momentum with gas, channelling it into the AGN's area of influence (Shlosman et al. 1989, Sellwood 2014), there is, however, no wide consensus on this. Although bars in the nuclear disc have only been identified in galaxies that already host a bar in the main disc, there is no evidence as yet to suggest that they are coupled (Corsini et al. 2003).

Processes that occur on galactic scales, even relatively violent ones such as major mergers, are not observable in any meaningful way over many human lifetimes; these events take place over the course of hundreds of millions, if not billions, of years (Schiavi et al. 2020). The use of computational methods is therefore an essential part of understanding how galaxies evolve. Simulations can be run for the length of time that suits the research question best, up to the lifetime of the universe. This gives the opportunity to follow the evolution of galaxies, from their formation to the present day. N-body simulations are defined in Binney & Tremaine (2008) as "programs that follow the motion of a large number of masses under their mutual gravitational attraction", the simulations I present include both gravity and hydrodynamic forces. Their use can give insight into the circumstances under which bars form and how their properties develop over time. Results from simulations can be compared to observational data to reveal any discrepancies between theory and reality.

At the genesis of N-body simulation studies, when the number of particles available was many orders of magnitude fewer than today, it was found that isolated discs quickly became unstable and formed strong bars (Miller & Prendergast 1968, Hockney & Hohl 1969, Hohl 1970). As a significant fraction of discs in the real universe when observed do not host a bar, there was a clear question: what is the mechanism which can stabilise discs against the formation of a bar? One solution came in the form of a massive halo, which when added to N-body simulations suppressed bar growth and promoted disc stability. The halo acts to stabilise the disc and impedes the formation of a bar (Ostriker & Peebles 1973). When a halo was first implemented into simulations it was 'rigid', meaning that its density distribution is constant over time (Berman & Mark 1979). Growth in bar length and bar strength was found to be suppressed when a massive rigid halo is present. However, the paradigm subsequently shifted again with the introduction of a 'live' cold dark

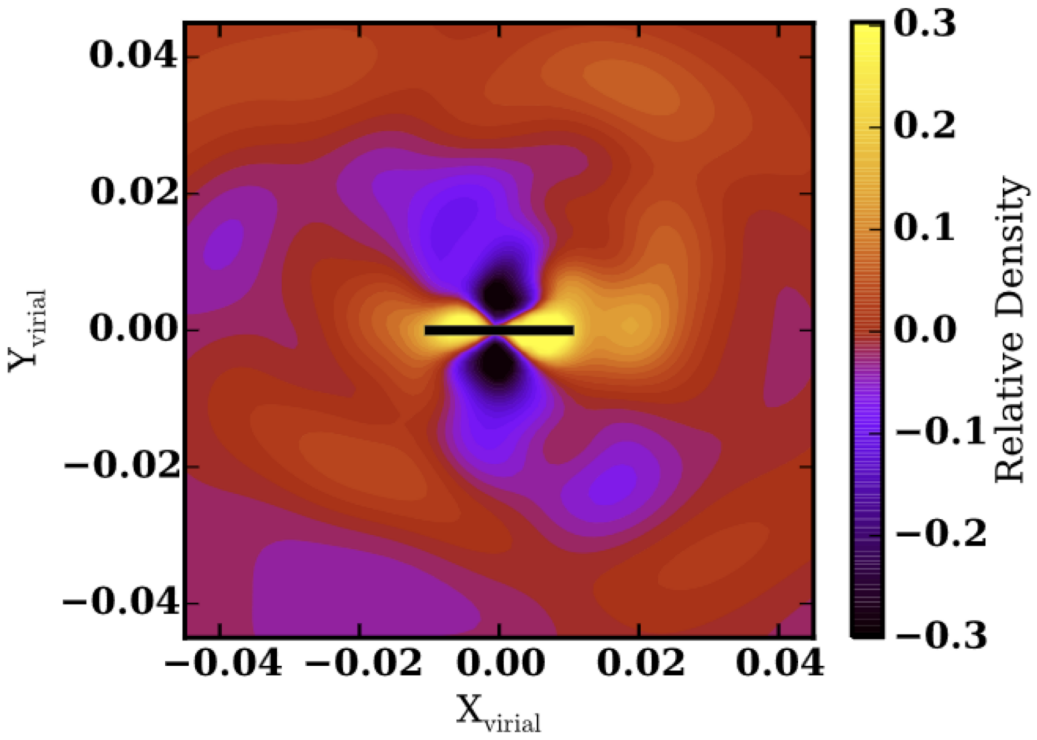

Figure 1.1: A dark matter wake following the bar in the halo of a simulated galaxy. The length and position of the bar is indicated with a straight black line. Here, with the bar rotating clockwise, dark matter lags behind the bar at radial distances greater than half the bar length, but generally aligned with the bar within this range. Positions are given in virial units. Reproduced from Petersen et al. (2016).

matter (CDM) halo that interacts other components of the galaxy. As shown in Athanassoula (2002), live halos whose mass is comparable to that of the disc can instead promote bar growth.

1.2 Bar Slowdown

The angular rotation speed of the bar, commonly referred to as the pattern speed, Ω_p, has been found to depend strongly on the distribution of dark matter in the central region of the galaxy (Debattista & Sellwood 2000). How matter in the galaxy is distributed determines the amount of material available to absorb or emit angular momentum at any given time. A bar slows down if it emits a significant amount of angular momentum, which can happen via two distinct mechanisms (Debattista & Sellwood 2000, Athanassoula 2003).

The first slowdown mechanism involves the elongation of bar supporting orbits. Stars can become trapped in orbits within a family that make up the backbone of

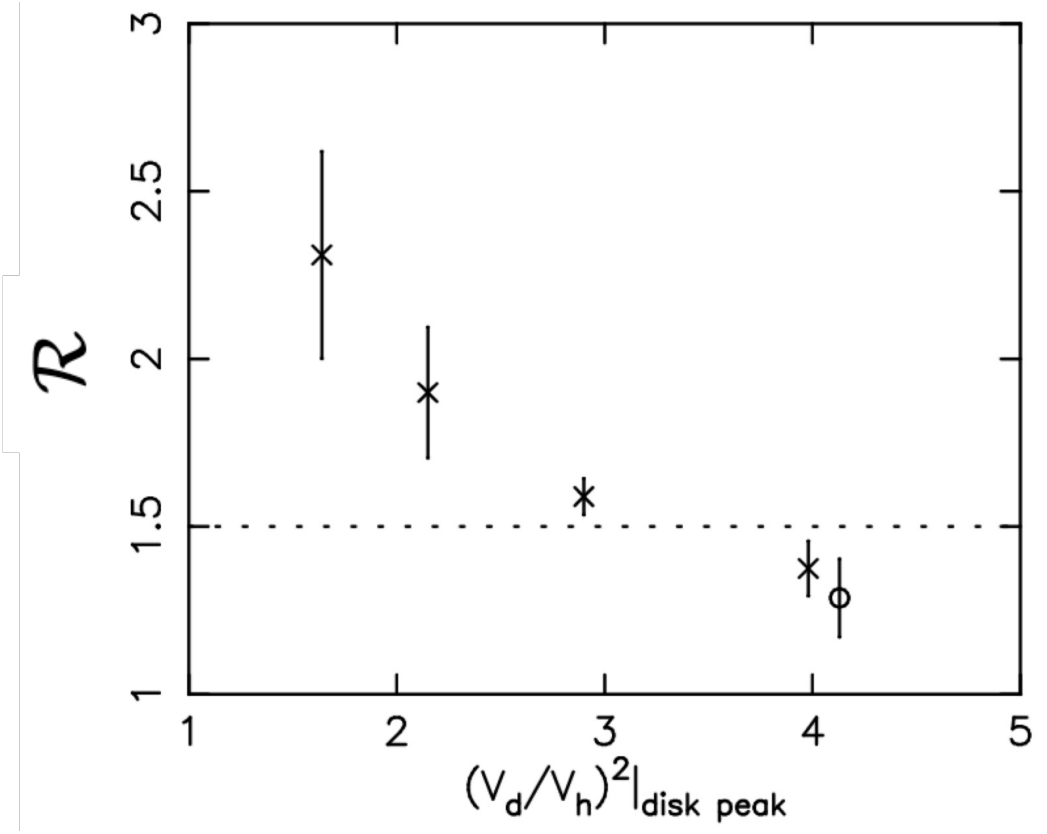

Figure 1.2: $\mathcal{R}$ against the disc to halo mass ratio squared taken at the peak value. It is clear from this plot that increasing the disc mass relative to the halo mass increases the speed of the bar in an isolated halo simulation. Adapted from Debattista & Sellwood 1998.

the bar's structure, named the x_1 family of orbits. When the disc emits angular momentum through exchange with the halo, this forces x_1 orbits to become more elongated with the effect of increasing the length of the bar ($R_{\rm bar}$) and decreasing its pattern speed (Athanassoula 2003).

The interaction between the bar and the halo via dynamical friction (Tremaine & Weinberg 1984b, Weinberg 1985) is the second mechanism by which a bar can slow down. Dynamical friction, first introduced by Chandrasekhar 1943, occurs when a large object travels through a field of less massive objects. As illustrated in Fig. 1.1, the gravitational attraction of the smaller objects forms a 'wake' that follows the larger object. Eventually, the wake is large enough to so that the gravitational drag force it exerts in opposition to the motion of the original mass is great enough to effect it on a Hubble timescale. In the context of the interaction between a dark matter halo and a bar, it is an angular version of dynamical friction in which the halo exerts a torque on the bar, causing $\Omega_{\rm p}$ to decrease. Unlike the first mechanism, this process does not necessarily proceed in tandem with a proportional increase

in $R_{\rm bar}$(Debattista & Sellwood 2000).

A dimensionless rotation parameter is often used in dynamical studies of bars and is defined by the ratio $\mathcal{R} \equiv R_{\rm CR}/R_{\rm bar}$, where $R_{\rm CR}$ is the corotation radius, the distance at which particles on circular orbits have an angular speed equal to $\Omega_{\rm p}$. This ratio is used to distinguish between the two slowdown mechanisms, as well as enabling comparison between galaxies of different sizes. As the bar slows down, $R_{\rm CR}$ extends further into the outer regions of the galaxy, increasing the value of $\mathcal{R}$. A lower limit of 1 was placed on $\mathcal{R}$ by theoretical work that concluded that the bar cannot extend beyond corotation (Contopoulos 1980).

It is often assumed that when bars form, they fill their corotation radius (Weinberg 1985,Frankel et al. 2022). By definition, this gives them an initial $\mathcal{R}$ of 1. Depending on how significantly they are slowed by dynamical friction, $\mathcal{R}$ will increase over time. As both mechanisms for bar slowdown act simultaneously, the $\mathcal{R}$ parameter gives insight into which is more prevalent. If the dominant slowdown mechanism is the elongation of orbits, $\mathcal{R}$ stays close to 1, else dynamical friction is dominant and the value of $\mathcal{R}$ increases. A widely used definition of 'fast' and 'slow' bars comes from Debattista & Sellwood (2000), who set boundaries on the fast bar regime at $1 \leq \mathcal{R} \leq 1.4$. The slow regime includes any bar for which $\mathcal{R} > 1.4$. In both observations and simulations, there have been bars measured as 'ultrafast' with $\mathcal{R} < 1$. As bars are unstable past this limit and would dissolve (Contopoulos & Grosbol 1989), it is thought that bar length measurements have been overestimated in cases where an ultrafast bar has been identified (Cuomo et al. 2021).

There have been plenty of studies that use isolated halo simulations in pursuit of understanding why bars slow down. One significant finding is that the distribution of dark matter in the central region of the halo is associated with whether a bar will slow down, and to what extent. In Debattista & Sellwood (1998), they show that a greater baryon dominance in the central region of the galaxy can act to reduce the effect of dynamical friction, as seen in Fig. 1.2. The definition of baryon dominance they use is the square of the peak disc to halo ratio of circular velocity. Baryon dominance acts as a proxy measure for the overall enclosed mass ratio between stars and dark matter in a defined region. The amount of dynamical friction exerted by the halo depends on both the mass of the particles associated with the bar (stars in bar supporting orbits) and the background density (i.e. the density of dark matter in the halo) (Sellwood 2006). We expect a galaxy that is more dominated by baryons to have a weaker overall effect from dynamical friction, resulting in less bar slowdown.

Factors other than the baryon dominance have been suggested to play a role in the slowdown of bars. For example, recent work done by Beane et al. (2023) focuses

on the gas fraction in the disc. In their isolated halo simulations, an idealised N-body simulation without gas shows a bar whose pattern speed decreases over time due to the effect of dynamical friction. They find that as the bar slows down, the main bar resonances move outward, increasing the amount of resonant material that can form the dark matter wake. Any additional material in the wake adds to the gravitational torque that opposes the motion of the bar, slowing it down. They then rerun the simulation, adding more gas to the disc with each iteration. When the gas fraction is 20%, the torque from dark matter reduces almost to zero and the bar experiences only a small slowdown. This suggests that the amount of gas in the disc can have a significant impact on whether the bar will end up being slow by $z = 0$. It is important to note, however, that their work only looks at how Ω_{p} evolves over time and is affected by gas, rather than the $\mathcal{R}$ parameter.

Athanassoula (2003) shows that the slowdown of the bar depends on the exchange of angular momentum between the disc and the halo components of the galaxy. As angular momentum is transferred from the disc to the halo, the bar strength grows and at the same time its pattern speed decreases. Orbits that support the bar structure are associated with the Inner Linblad Resonance (ILR) i.e. they satisfy the equation $l\kappa + m\,(\Omega - \Omega_{\mathrm{p}}) = 0$ for (m,l) = (1,2), where κ is the epicyclic frequency, Ω the angular speed of the star and Ω_{p} the pattern speed of the galaxy. it is these same orbits that are most able to exchange angular momentum with resonant material in the halo.

An additional factor that can affect the ability of the halo and disc to exchange angular momentum is the velocity dispersion of either component. Athanassoula (2003) also explores how changing the velocity dispersion in the disc can affect slowdown. The Toomre Q parameter is used to describe a disc as 'hot' or 'cold', with Q defined as

$$Q = \frac{\sigma_{\mathrm{R}}\kappa}{3.36G\Sigma} \tag{1.1}$$

where σ_{R} is the radial velocity dispersion, κ the epicyclic frequency, G is Newton's gravitational constant and Σ is the surface density (Toomre 1964). A greater value of Q indicates a hotter disc. From the coldest to the hottest discs, there is a vast difference in bar slowdown, with the coldest experiencing more than four times the slowdown rate. In the halo component, velocity dispersion also plays a significant role in how much the bar slows down. A cold halo can absorb much more angular momentum than a hot one and greater angular momentum exchange is directly linked to increased bar slowdown. The bar itself will have a large influence over the velocity dispersion in the bar region, so it is difficult to draw conclusions about

hot and cold discs in this area. At distances greater than the bar length, we would expect that if a disc is hotter, the bar should experience less slowdown due to a decrease in the exchange of angular momentum between the disc and halo components.

Another study focuses on the relationship between the 'spin' of the dark matter halo and the galactic bar. Spin is defined as the angular momentum of the halo normalised by the maximum allowed angular momentum. Li et al. 2023 explores the parameter space of spin and halo density simultaneously. They find that a low density, high spin halo can stabilise the bar and lead to decreased torque from the halo, resulting in reduced bar slowdown. When the halo is given zero, or low, initial spin there is a greater difference in the angular momentum of dark matter and stellar components. This gap leads to more angular momentum exchange between the bar and halo, each exerting a torque on the other. The halo gains angular momentum as the bar loses it. As the bar's angular momentum decreases, so does its $\Omega_{\rm p}$. On the other hand, if the halo starts with some angular momentum, it will not torque the bar as strongly, resulting in reduced bar slowdown. Dark matter halo spin has not been thoroughly investigated in a cosmological context.

The studies presented in this section have so far all used isolated halos. In these the disc properties are set as part of the initial conditions of the simulation and galaxies do not form in the cosmological context. While they provide useful data for understanding the interaction between different galactic components, cosmological simulations allow us to make direct comparisons with observed data.

1.3 Tension in bar properties between Observation and Simulation

Two relatively recent developments have allowed for the study of the $\mathcal{R}$ parameter in observations and simulations. Kinematic data from large Integral Field Unit (IFU) surveys has allowed the measurement of $\Omega_{\rm p}$ in a growing number of observed galaxies. A little over a decade ago only a handful galaxies had reliable pattern speed measurements (e.g. Corsini 2011, Aguerri et al. 2015, Williams et al. 2021, etc.). Since then, large surveys such as MaNGA (Bundy et al. 2015) have provided data which has expanded the number of known $\Omega_{\rm p}$ values to almost 100 (Schmidt et al. 2023). On the theoretical side, cosmological simulations with improved resolution have produced large populations of barred galaxies from which $\mathcal{R}$ can be determined (e.g. Algorry et al. 2017, Roshan et al. 2021). Comparing the rotation parameter, $\mathcal{R}$, in simulations and observations provides a good test of whether sim-

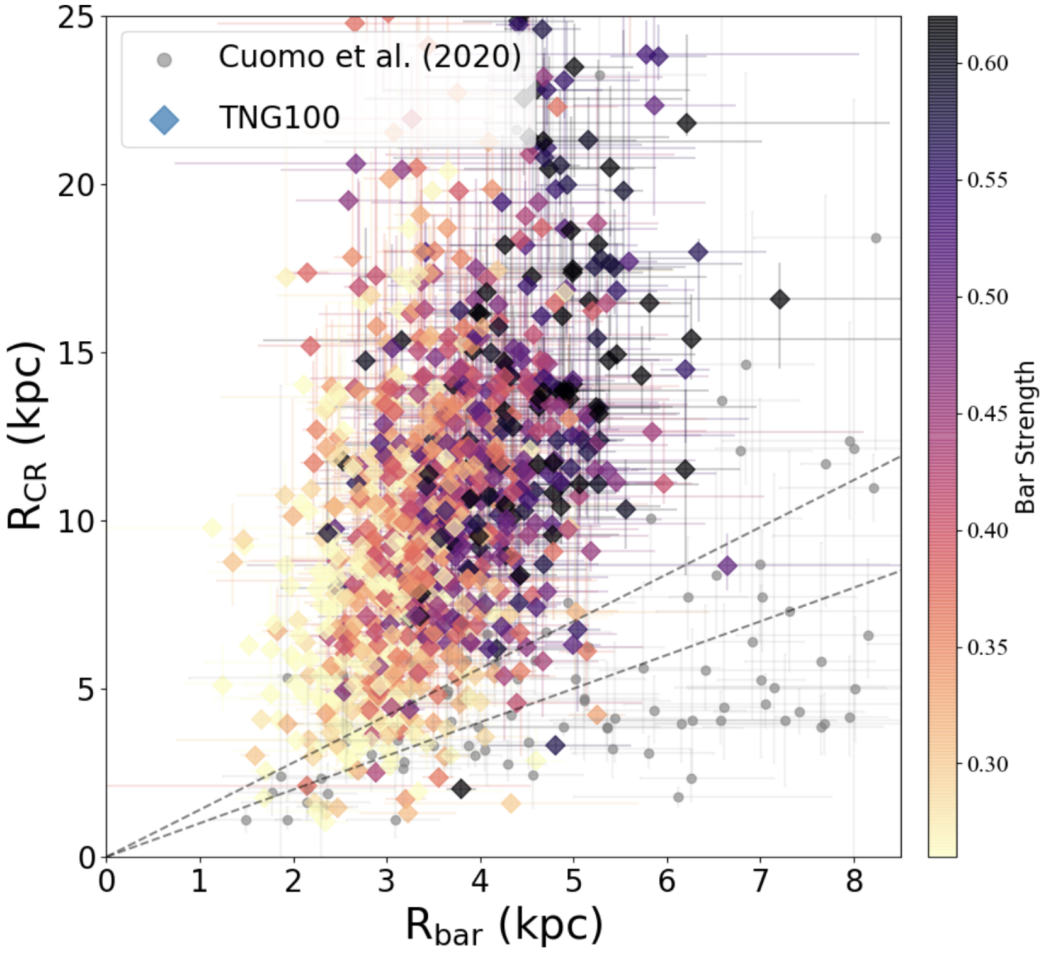

Figure 1.3: Relation between the bar length and the corotation radius for galaxies produced in the IllustrisTNG100 simulation at $z = 0$ (diamonds) compared with observational data (circles) taken from Cuomo et al. 2020. Dashed lines indicate the boundaries of the fast bar regime at $\mathcal{R} = 1$, 1.4. The colour of the diamonds indicates the strength of the bar at $z = 0$, with darker shades signalling a stronger bar. Adapted from Roshan et al. 2021.

ulations are producing a realistic picture of the universe and whether the current leading cosmology, ΛCDM, is correct, assuming that the subgrid physics correctly models galaxy formation in this cosmology.

Studies of observed galaxies find that in the local universe bars tend to rotate fast (Aguerri et al. 2015, Cuomo et al. 2020). Similar analysis performed on cosmological simulations find that by $z = 0$ bars tend to be slow (Algorry et al. 2017, Peschken & Łokas 2019). Fig. 1.3, reproduced from Roshan et al. (2021), shows the relationship between bar length and corotation radius in the TNG100 simulation as well as data from observation (Cuomo et al. 2020). The coloured diamonds represent simulated galaxies, a significant proportion of which lie in the slow bar region of the plot. Observational data is shown with grey circles and, in contrast to the simulated points, are either within or below the dashed lines, in other words, these galaxies are fast. In Roshan et al. (2021), they find that measuring $\mathcal{R}$ in the same way for observed and simulated galaxies produces results that are incompatible with one another. Between their results for TNG100 and observation they calculate a tension of $\sim 12\sigma$. This poses the question, can galaxies in ΛCDM produce fast bars at $z = 0$? If they cannot, there is a tension between theory and reality.

In Frankel et al. (2022) the $\mathcal{R}$ value in bars from the TNG50 simulation is compared with a sample of observed galaxies from the MaNGA survey (Bundy et al. 2015). They too find that the value of $\mathcal{R}$ is greater in the simulated galaxies. Frankel et al. suggest that the differences arise from a difference in the bar length rather than in the pattern speed. While the two sets of data show similar pattern speeds, the TNG50 bars are much shorter, and therefore are 'slower' in the sense of having a greater $\mathcal{R}$.

Fragkoudi et al. (2021) uses the Auriga suite of cosmological zoom-in simulations (Grand et al. 2017) to explore the pattern speed of bars. Zoom-ins are a rerun of a big box cosmological simulation with a greater resolution for the particles in a chosen halo, and decreased resolution for the rest of the box. This is advantageous for studying single galaxies at a greater resolution while preserving their formation history within the cosmological context. Degrading the resolution outside the area of interest makes outputting data frequently throughout the simulation less computationally expensive, an essential for studying dynamics. Fragkoudi et al. (2021) found that barred galaxies in Auriga remain fast, down to $z = 0$. This provided evidence in support of fast bars existing within ΛCDM cosmology. While this answers one question about the slow bar problem, it does raise another: why do bars stay fast in some simulations (Auriga) and slow down significantly in others (EAGLE, IllustrisTNG)?

So far there have been a few proposed solutions to this problem, for example Roshan et al. (2021) argues that theories of modified gravity can provide fast bars at $z = 0$, while ΛCDM cannot. However, there is insufficient evidence to rule out ΛCDM as it has been shown predictions from simulations using ΛCDM can change depending on, among other factors, the resolution, and the subgrid physics model employed by a simulation. The definition of resolution in simulations relates to the mass and number of particles of dark matter, stars, and gas. There have been numerous studies on the effect that the level of resolution in a simulation has on discs and their substructures, with divergent conclusions (e.g. Weinberg 1998, Valenzuela & Klypin 2003, etc.).

In the work by Fragkoudi et al. (2021), they carry out a investigation as to what effect the resolution of their simulations had on their results, some of the galaxies were rerun at a lower resolution than the original Auriga zoom-ins. This was done in order to explore whether lower resolution would lead to slower bars, thus bringing the results into agreement with previous findings from the EAGLE and Illustris simulations. As there was only a slight change in the value of $\mathcal{R}$, they concluded that differences in the subgrid physics was the main driver for the differences in the bar pattern speed. The subgrid physics model is the part of the code that deals with mechanisms that occur below the simulation's resolution limit. Many baryonic processes, such as feedback from supernovae and AGN, fall into this category. Using a different subgrid physics model will have a large effect on the baryonic components of the galaxy.

Evidence for an opposing viewpoint, that resolution is the underlying cause of slow bars, was provided by Frankel et al. (2022). This work uses the TNG50 simulation to test if resolution can have an effect on the bar speed. After rerunning their original simulation and degrading the mass resolution by a factor of eight, they find that bars on average have a lower pattern speed in the low resolution run, and a higher average value of $\mathcal{R}$. The question of which factor, resolution or subgrid physics, is the most important for the differences in $\mathcal{R}$ found between large box and zoom-in simulations is therefore still unanswered. It is also worth noting that changing resolution can have different effects depending on the subgrid model, a good test would be to compare subgrid models at the same resolution.

1.4 Aims of this Work

The central questions of the project are these: does the subgrid physics model of a simulation have an effect on the bar speed? In which ways are the global properties of a galaxy affected by the subgrid regime? How do these properties then relate

to $\mathcal{R}$? My work aims to answer these questions by analysing the effect of subgrid physics on barred spirals in zoom-in cosmological simulations. To investigate this I require a set of simulations that are identical aside from the subgrid model. They should be run with the same cosmology and at the same resolution for the same amount of time. I have taken Auriga galaxies that host bars at $z = 0$ and rerun them with the same resolution, initial conditions and cosmology but using the TNG subgrid model. While I am mostly interested in how the final $\mathcal{R}$ parameter changes under these circumstances, this exercise provides an opportunity to assess the difference in global properties of barred galaxies and discuss how the differing subgrid models bring about any contrast in characteristics.

The rest of my work is structured as follows: in Chapter 2 I describe the simulations and their subgrid models, as well as outlining how the analysis was performed on the halos. In Chapter 3 I present the results of the analysis, using an example of how one halo evolves over time in both models as well as examining the properties of the galaxy population at $z = 0$. I discuss the results within the context of the wider literature in Chapter 4 and make final conclusions in Chapter 5.

Chapter 2

Methods

2.1 Simulations

In this project I have analysed seven halos taken from the Auriga suite (Grand et al. 2017). Auriga is a set of thirty zoom cosmological magneto-hydrodynamical simulations and was run using the moving-mesh code AREPO (Springel 2010). The virial mass definition used in Auriga is M_{200}, the mass contained within a radius at which the mean enclosed mass density equals 200 times the critical density for closure. Dark matter particles have a mass of $3 \times 10^5 \mathrm{M}_\odot$ and the initial baryon resolution is $5 \times 10^4 \mathrm{M}_\odot$. Compared to EAGLE the mass resolution in Auriga is an increase of more than an order of magnitude in both components. The cosmological parameters for the simulations were $\Omega_m = 0.307$, $\Omega_b = 0.048$, $\Omega_\Lambda = 0.693$ and $\mathrm{H}_0 = 100h$ kms^{-1} Mpc^{-1}, where $h = 0.6777$, taken from Planck Collaboration et al. 2014. I employ these same parameters for the re-simulations of the Auriga halos using the TNG subgrid model.

The initial conditions for the Auriga halos are extracted from the 100cMpc (co-moving megaparsecs) box generated by the EAGLE (Evolution and Assembly of GaLaxies and their Environments) Project (Schaye et al. 2015). EAGLE is a set of cosmological simulations with various box sizes, the largest of which is 100cMpc. Within the box are many thousands of galaxies, only some of which have discs. The halos selected are Milky Way-sized late type galaxies, meaning they have a mass range of $1 - 2 \times 10^{12}$ $\mathrm{M}_\odot$. Many of the thirty Auriga galaxies host bars at $z = 0$ (e.g. Fragkoudi et al. 2020).

A zoom simulation is a rerun that preserves all the same cosmological context as found in the original simulation but increases the resolution around a given region of interest. For my own work, greater resolution allows me to analyse bar properties in more detail than would otherwise be possible. Cosmological simulations capture

the formation and growth of a galaxy self-consistently. Being produced in this way is why we can compare galaxies in zoom simulations to observed galaxies in the real universe. Auriga halos reproduce many of the same properties as we see in observation, such as the Tully-Fischer relation (Grand et al. 2017). TNG galaxies have also been shown to reproduce this relation between mass and rotation velocity (Goddy et al. 2023).

For dynamical studies it is advantageous to have simulations that output data as frequently as possible. The original Auriga runs have 127 full snapshots, outputs of all the particles in the simulation at a given time. As this is insufficient for my analysis I have made use of higher cadence reruns that produced 251 full snapshots as well as 2763 so called 'snipshots' that only output data for the stellar particles. At low redshift ($z < 1$), the time step between each full snapshot is ~65 Myrs; the gap between each snipshot is much smaller, around 5Myrs. I used the same number of snapshot and snipshots when running the simulations with the TNG subgrid model (Weinberger et al. 2017, Pillepich et al. 2018, Nelson et al. 2019, Pillepich et al. 2019).

Both the original Auriga and my own simulation are run using the magneto-hydrodynmical simulation code AREPO (Springel 2010). Initial conditions and resolution are also the same for the simulations using the TNG subgrid physics as they are for the Auriga halos. The similarities and differences of the two models I describe below.

Substructures are identified in the simulations using the SUBFIND (subhalo finder) algorithm (Springel et al. 2001), which categorises a self-bound overdensity within a background Friends of Friends (FoF) group as a subhalo. The centre of this subhalo is defined as the position of the most bound particle, defined using the particles' gravitational potential only. Using merger trees, the subhalo that I study at $z = 0$ can be traced backwards in time so that its dynamical evolution can be observed.

2.2 Subgrid Modelling

The main motivation for this project is to analyse the effect that subgrid physics models have on the properties of galaxies which are relevant for the slow down of stellar bars. I will briefly outline the differences in the baryon physics models used by Auriga and TNG. For full technical details of these models, see Grand et al. 2017 (Auriga), Pillepich et al. 2018 and Weinberger et al. 2017 (TNG).

The two physics models bear many similarities, one of which is how they model star formation and the interstellar medium (ISM). Both follow the method first introduced in Springel & Hernquist 2003. For primordial and metal-line gas cooling, Auriga and TNG are identical, using the prescription outlined in Faucher-Giguère et al. 2009 and Pillepich et al. 2018. The way in which each deals with galactic winds however, is different. These winds are a consequence of supernovae events, both type Ia (SNIa) and II (SNII). In the Auriga and TNG models, these events involve converting a star-forming gas cell into a 'wind' particle. These particles are then launched isotropically (in a random direction) with velocity proportional to the local one-dimensional dark matter velocity dispersion (e.g. Okamoto et al. 2010). The feedback from both SNIa and SNII make up a meaningful part of the feedback injected into the ISM and consequently affect the amount of star formation going on at any one time during galactic evolution. If there is a greater amount of feedback, the gas in the disc has an increased velocity dispersion, and is less dense. The knock on effect of this is reduced star formation in the disc and eventually the quenching of galaxies. While the implementation of wind is the same in Auriga and TNG, the parameters they use differ slightly and as a result the winds in TNG are stronger than those in Auriga.

The main area that the two models differ significantly is in their treatment of feedback from active galactic nuclei (AGN). Modelling feedback from AGN is an active area of debate (e.g. Huško et al. 2024, Eckert et al. 2021, etc.) as much of the processes that occur in the regions close to AGN are the subject of open questions. Both Auriga and TNG follow a 'two-state' model; creating separate feedback provisions for states of high and low accretion in the AGN. In the high accretion state (the so called quasar mode) they model feedback in a similar way, injecting thermal energy into the ISM around the AGN, albeit with slightly different thermal coupling efficiency in the surrounding gas. The low accretion state (radio mode) is where they diverge substantially; the feedback from AGN in TNG is purely kinetic, giving surrounding gas cells a kinetic 'kick'. Auriga, in contrast, models feedback in the radio mode as thermal, heating bubbles of gas isotropically around the AGN (Grand et al. 2017, Weinberger et al. 2017, Pillepich et al. 2018). The object of this work is not to make judgements on if either of these two models is the 'correct', rather, it is to observe and attempt to assess how subtle differences in subgrid physics can affect the dynamical properties of simulated disc galaxies.

2.3 Halo Selection

Part of the selection criteria for the halos in Auriga is that they are in relatively isolated FoF groups $z = 0$, isolation is determined by the amount of tidal force they experience from neighbouring groups. This increases their value to my work as there are no major external factors influencing the speed of the bar at the end of the simulations. Halos are selected to be rerun with TNG physics if they host a bar at $z = 0$. Of the set of thirty Auriga galaxies, seven were chosen to be rerun using TNG physics. If a TNG rerun does not host a bar at $z = 0$, it was excluded from the analysis, as the goal was to compare the bar pattern speed of galaxies in simulations with the TNG and Auriga model. The question of how the physics models of these two suites affect the formation of bars is an interesting one in itself, but is beyond the scope of this work. The five halos from the Auriga suite that are included in the final analysis are Auriga 2, 9, 17, 18 and 22.

Throughout the rest of my thesis I employ the following nomenclature when referring to galaxies, the subgrid model followed by the halo number as given in Grand et al. 2017. For example, Auriga 18 (Au18) is halo 18 from the Auriga suite and TNG18 refers to the rerun of Au18 using the TNG subgrid model.

2.4 Analysis

To determine the effect of subgrid physics on the speed of bars, I make measurements of key characteristics over the course of the simulation. Observational studies are limited to analysing the pattern speed of bars in the local universe, at $z = 0$. I therefore focus on the properties of my galaxies at this time. Merger trees were used to trace the main halo throughout the simulation so that its evolution could be analysed. Each time a halo was loaded, before I perform the following analysis, the galaxy is centered on the origin. To align the disc I use the angular momentum vector of the stars in the central 30kpc and rotate the box such that this vector is normal to the x-y plane.

I define the stellar mass of the galaxy as the stellar mass within the central 30kpc, with a vertical cut of +/- 1kpc. This area captures the entire disc but is small enough to include material only in the subhalo of interest. When measuring different properties, the vertical region is not always 1kpc within a range $0.8kpc < |z| < 2kpc$. This is to fit in with the same measurements made in different studies, overall the choice in perpendicular direction makes only a small difference.

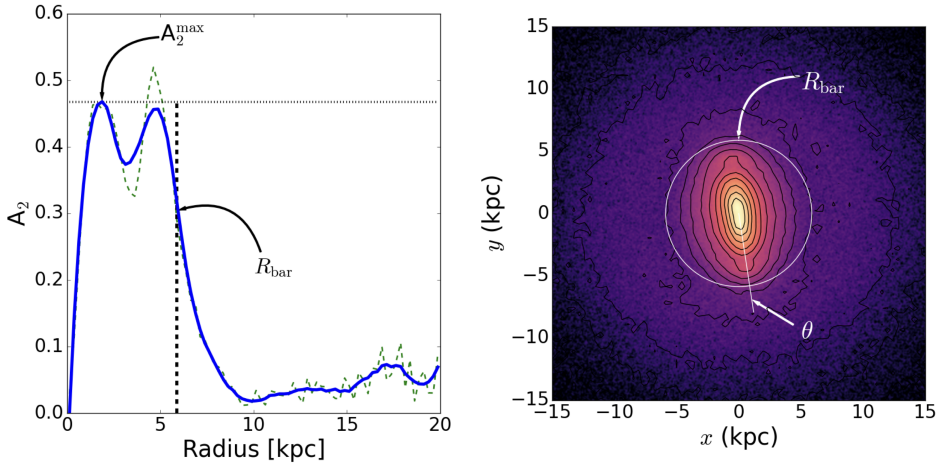

Figure 2.1: *left*: A_2 against radius for the final snapshot of Au17. The arrows show the value of A_2^{max} at the first peak and R_{bar} at the radius where $A_2 = 0.65A_2^{max}$. The green dashed line is the A_2 before smoothing. *right*: A surface density plot of the x-y projection of the stars from the same snapshot. The white circle has a radius R_{bar} and the white line shows the phase angle of the bar ($\langle\theta\rangle$). The length of the line is arbitrary.

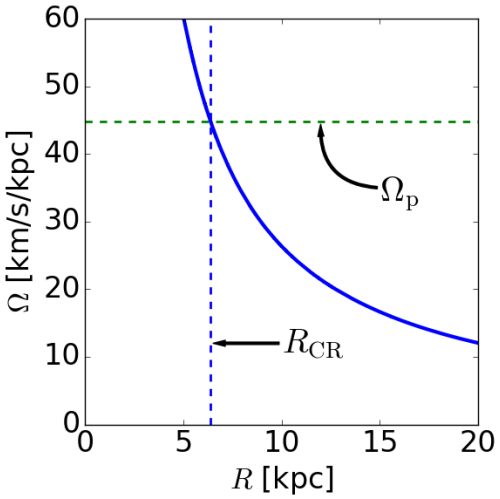

Figure 2.2: The frequency of circular orbits in the final snapshot of Au17 as calculated with Eq.2.7. The horizontal line is the pattern speed and where this intersects with the curve is the corotation radius.

Due to the large number of simulation outputs, it is advantageous to be able to carry out the analysis on the bar length, strength and pattern speed automatically. However, the methods were checked by eye to ensure accuracy, especially at times that are important for analysis, most notably the final snapshot at $z = 0$.

2.4.1 Bar Strength

I define the bar strength as the first peak in the normalised m = 2 Fourier mode of the surface density within 8kpc of the galactic centre. I used stellar particles in the disc, i.e. $|z|$ <0.8 kpc, in annuli of width 0.25 kpc to measure,

$$a_m(R) = \sum_{i=0}^{N-1} \mathrm{m}_i \cos(m\theta_i), \quad m = 0,1,2,... \tag{2.1}$$

$$b_m(R) = \sum_{i=0}^{N-1} \mathrm{m}_i \sin(m\theta_i), \quad m = 0,1,2,... \tag{2.2}$$

where m_i is the mass of particle i, R is the cylindrical radius, θ is the azimuthal angle and N is the total number of particles. I then use the ratio

$$\mathrm{A}_2(R) = \frac{\sqrt{a_2^2 + b_2^2}}{a_0} \tag{2.3}$$

as the normalised m = 2 Fourier mode of the surface density. This is smoothed with a Savitzky-Golay filter, window length 15 snipshots and polynomial order 3, and the bar strength ($\mathrm{A}_2^{\mathrm{max}}$) is the first peak of the smoothed A_2 vs radius distribution. The window length of 15 is for simulations that have stellar only snipshot outputs, for other simulations the filter was adjusted proportionally to the number of simulation outputs.

Fig. 2.1 shows an example of how the bar strength is measured for one of the halos in our sample, Au17. In some cases the A_2 vs R plot can show a double peaked distribution, as in the Fig. 2.1. I use a peak finding algorithm to identify all peaks in the distribution, and then select the first one to be the bar strength. Using this each time makes automating the analysis more straightforward. In some cases, any peaks after the first are caused by additional galaxy features outside of the bar (e.g. spiral arms). For the example shown in Fig. 2.1, both peaks come from different areas of the bar, but have similar $\mathrm{A}_2^{\mathrm{max}}$ values, so choosing one over the other has little effect on the value of $\mathrm{A}_2^{\mathrm{max}}$. I use the definition that a galaxy is barred if $\mathrm{A}_2^{\mathrm{max}}$ is greater than 0.25. As a result, the bar formation time is the final time that the $\mathrm{A}_2^{\mathrm{max}}$ is measured to be below this threshold.

2.4.2 Bar Length

There are many different ways to define the length of a galactic bar. Examples of methods often used in observational studies include isophotal ellipse fitting (e.g. Erwin 2005) or analysis of the m = 2 Fourier mode (e.g. Athanassoula & Misiriotis 2002), among others (e.g. Wegg et al. 2015, Wu et al. 2018, Hilmi et al. 2020). When analysing the bar length in observation and simulation it is important that we are making apples to apples comparisons, which can only be achieved if the same definition of bar length is used. In my work, I am more concerned with being able to easily automate the process of measuring bar length across thousands of snapshots. As long as I am able to make apples to apples comparisons within my own galaxy selection, the effect of the subgrid physics model can be seen. However, these results should not be compared directly to observations, since the bar length I use is not the same as those commonly used in observations. A summary of a number of methods used in simulations to measure bar length is presented in Ghosh & Di Matteo 2023. A new method that analyses the orbital structure of a galaxy in order to measure the length of the bar can be found in Petersen et al. (2023).

I explored different ways of calculating the bar length in the simulations. The first defines the bar length as the extent to which the phase angle of the m = 2 Fourier mode remains constant within a given phase tolerance. In my tests, I employed tolerances of 3, 4 and 5 degrees as the cutoff. This method is easy to automate over many snapshots, which made it an attractive prospect. However, this method produced data that was too noisy to be useful. The bar length changed significantly from snapshot to snapshot in a way that was not consistent when making comparisons visually with surface density plots. While this was the main reason for discarding the phase angle method, it also consistently over measured the bar length for all tolerance values.

The alternate method I considered defines bar length as the radial extent at which the bar strength drops to a certain proportion of the peak value. As with the previous method this was straightforward to automate. After testing different values, I found that taking the bar length at the distance when the A_2 value drops to 65% of $A_2^{\max}$ generally matched the visual length of the bar, and produced data that were far less noisy than the phase angle method. As with measuring $A_2^{\max}$, non-bar features that contribute power to the m = 2 Fourier mode can interfere with bar length measurements (Hilmi et al. 2020), most often the effect of this is to artificially extend the length.

I do not employ the same method for measuring bar length as in observations because I want to use a method that is more easily automated. Using the same

method across all my halos allows me to compare between different simulated galaxies reliably. Fig. 2.1 shows how $A_2^{\max}$ and $R_{\rm bar}$ are recovered from a single snapshot in Au17. The left panel shows an A_2 vs R plot with $A_2^{\max}$ and $R_{\rm bar}$ labelled, the right panel shows a surface density plot of this same snapshot. The white circle in the x-y plane has a radius $R_{\rm bar}$. This matches well with a visual estimate for the bar length.

2.4.3 Pattern Speed

To measure the pattern speed automatically over many simulation outputs, I measure the phase angle (θ) of the m = 2 Fourier mode

$$\theta(R) = 0.5 \ \mathrm{atan2}\left(b_2(R), a_2(R)\right) \tag{2.4}$$

where R is the cylindrical radius. Here I use the arctan2 function, which gives theta a range (when the factor of 0.5 is applied) on $0 \leq \theta < \pi$. For each snapshot, $\langle\theta\rangle$ is the average of this measurement inside 80% of the bar length. This region is chosen for the phase measurement as the m = 2 Fourier mode is less likely to be affected by non-bar features, such as spiral arms. Fig. 2.1 shows $\langle\theta\rangle$ as a white line of arbitrary length. The pattern speed is determined using

$$\Omega_{\rm p} = \frac{\Delta\langle\theta\rangle}{\Delta t} \tag{2.5}$$

where $\Delta\langle\theta\rangle$ is the difference in bar phase and Δt is the timestep between sequential snapshots. Similarly to $R_{\rm bar}$, measuring pattern speed this way means it is affected by any extra m = 2 components that rotate independently of the bar. Secondary bars, spiral arms and a nuclear disc (that can itself host a bar) are all features that may effect the measured $\Omega_{\rm p}$.

Of the ten galaxies that I analyse, five Auriga and five TNG, eight have high cadence outputs, meaning that the simulation outputs data at a high frequency. For these it allows analysis of the dynamical properties of the galaxy with only small time steps between each snapshot. Au2 and Au22, on the other hand, were not rerun in this way and as a result a different method of determining the pattern speed is required. When faced with low cadence outputs, or when using observational data, the most often used way to determine pattern speed is the Tremaine-Weinburg method (TW; Tremaine & Weinberg 1984a)

$$\langle V\rangle = \langle X\rangle \ \Omega_p \ \sin i \tag{2.6}$$

Where i is the disc inclination and

$$\langle X \rangle = \frac{\int X \Sigma dX}{\int \Sigma dX}, \quad \langle V \rangle = \frac{\int V_{\rm los} \Sigma dX}{\int \Sigma dX}$$

are the photometric and kinematic integrals, the luminosity weighted average positions of X (photometric) and the line of sight velocity $V_{\rm los}$ (kinematic), Σ is the surface density. This way of determining pattern speed is used in observations, and simulations with lower cadences, as it is fairly straightforward and relies on observable properties. In observational studies, the surface density is determined using a surface brightness and an assumed mass to light ratio. However, it does introduce three assumptions, first that the disc of the galaxy is flat (i.e. has zero thickness), that the bar has one well defined pattern speed, and that the tracer obeys the continuity equation. Using the TW method has been well tested in various observational and simulation studies (e.g. Aguerri et al. 2015,Cuomo et al. 2020, Garma-Oehmichen et al. 2022, etc.) Values of $\Omega_{\rm p}$ determined using the TW method are accurate to approximately 10% (Cuomo et al. 2020). On the galaxies which do not require the TW method, Fragkoudi et al. (2021) provides a helpful comparison as they do use the TW method to find $\Omega_{\rm p}$, with results that agree with my own. A way to use the TW method to find the pattern speed using only a single simulation snapshot was recently presented in Dehnen et al. (2023).

2.4.4 Corotation Radius

The definition of the corotation radius ($R_{\rm CR}$) is the radius at which stars on nearly circular orbits would have the same angular frequency as the bar. The first step in determining $R_{\rm CR}$ is to recover the rotation curve for the galaxy using

$$v_c^2 = \frac{GM(< R)}{R} \tag{2.7}$$

where G is the gravitational constant, $M(< R)$ is the enclosed mass and R is the cylindrical radius. This equation assumes a spherically symmetric system, Binney & Tremaine (2008) finds that v_c peaks at a value 15% greater in an exponential disc than Eq 2.7 and the two become closer at greater distances. As the peak for the galaxies I present is generally within 1kpc of the centre, this approximation works well for my purposes. The corotation radius is then defined by using the formula $\Omega_p R_{CR} \equiv v_c(R_{CR})$. Fig. 2.2 shows a visual example of how the corotation radius is determined. The shape of the curve indicates that a lower $\Omega_{\rm p}$ would result in a more extended corotation radius. Inside $R_{\rm CR}$ orbits have a greater angular frequency than $\Omega_{\rm p}$ and outside $R_{\rm CR}$ their angular frequency is less than $\Omega_{\rm p}$. As

the angular frequency of these orbits is dependent on enclosed mass, in a disc with greater mass the whole curve would move up. If two galaxies have the same Ω_{p}, the more massive disc has a longer R_{CR}.

Chapter 3

Results

In Section 3.1 I present the temporal evolution of the dynamical properties of one halo from the Auriga suite, run first with the fiducial Auriga and then the TNG subgrid physics model. This gives the opportunity to directly compare how a bar evolves between the two. In Section 3.2 the results for the full set of galaxies at $z = 0$ are introduced. This gives an overview of how the subgrid physics model affects the properties of the affects the properties of halos simulated with two different subgrid physics models.

3.1 Time Evolution of Halo 17

3.1.1 Bar Properties

In this subsection I present the temporal evolution of a number of dynamical quantities for Halo 17 from the original Auriga suite, and compare them to the same halo rerun with subgrid physics model from TNG. Throughout the results, time is given as lookback time ($t_{\rm lookback}$) from $z = 0$. At time moves forward, $t_{\rm lookback}$ decreases from left to right on the x-axis. To give a visual intuition for what these two galaxies look like I present Fig. 3.1 which shows surface density plots of the halo in both subgrid models at three snapshots. First the time at which the bar forms, then at a lookback time of 4Gyrs and finally at $z = 0$. Even without quantitative data, there are some clear differences between the two. At both the 4Gyr and $z = 0$ snapshot, the stellar disc in Au17 visually extends to a greater distance and its bar is longer than that of TNG17. The large number of contours towards the centre of TNG17 at $z = 0$ suggests that the galaxy has a larger central concentration of stars, compared to the fewer contours seen in the same region of Au17.

One feature of Au17 that is not present in TNG17 is a boxy-peanut bulge in the

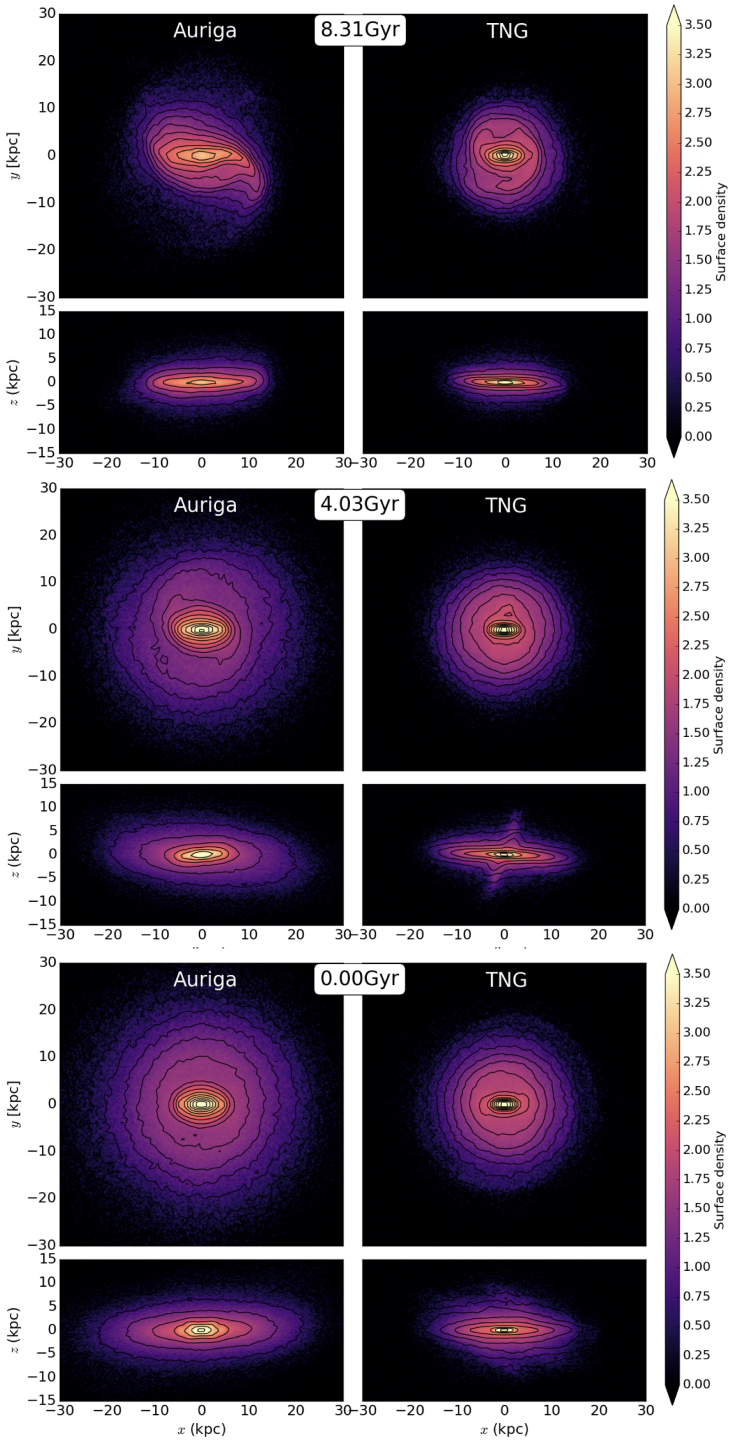

Figure 3.1: Surface density plots of the x-y and x-z projections of Au17 (left) and TNG17 (right) as they evolve from when the bar in Auriga 17 forms (top) to $z = 0$ (bottom).

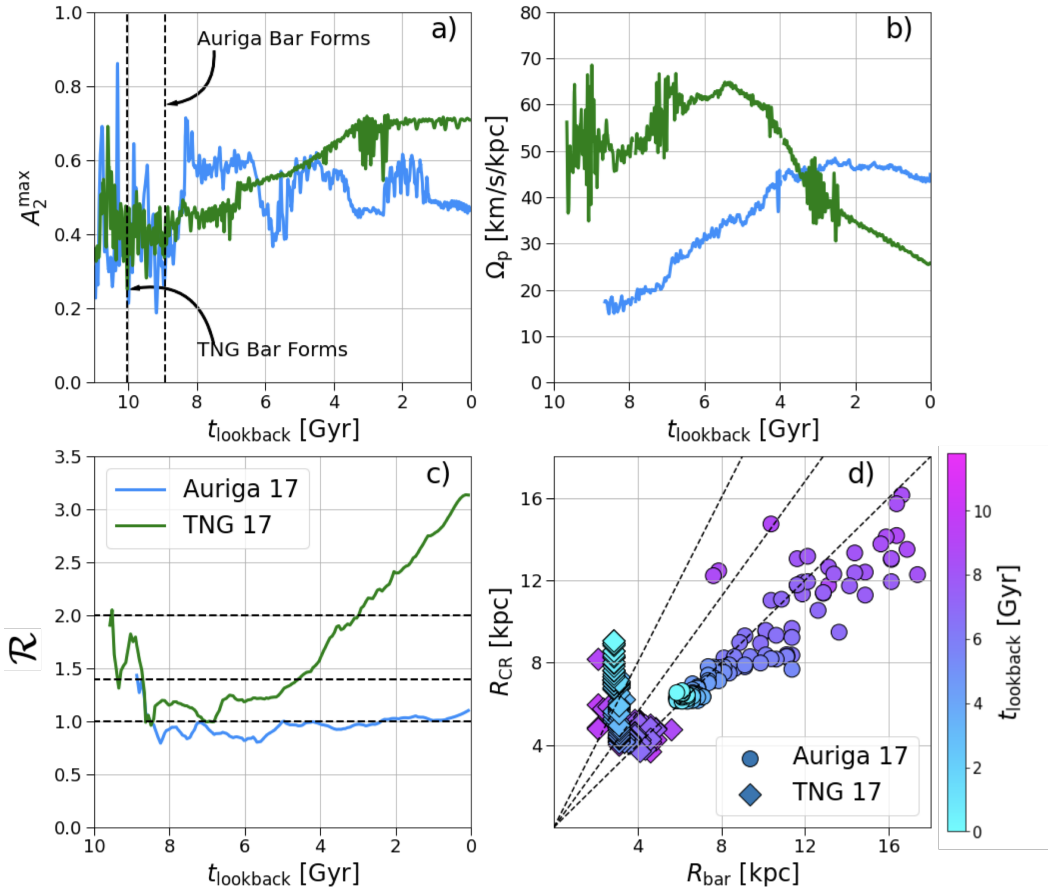

Figure 3.2: Time evolution of bar properties in Halo 17 in both the Auriga and TNG subgrid models. *a)*: The bar strength against lookback time. The bar formation time is shown here by vertical dashed lines. *b)*: The temporal evolution of the pattern speed plotted from the bar formation time of Au 17 and TNG 17. *c)*: The $\mathcal{R}$ parameter against time, with dashed lines at $\mathcal{R} = 1$, 1.4 and 2. *d)*: The bar length against the corotation radius, the colour of each marker maps to its lookback time. Dashed lines here show where the $\mathcal{R}$ value is constant, going anticlockwise they are at $\mathcal{R} = 1$, 1.4 and 2.

final snapshot. This can be identified visually by a characteristic X-shape towards the centre in the lower panel, the x-z projection. The presence of this bulge in one galaxy and not the other is an early indication that the subgrid physics do have a measurable effect, even without making quantitative measurements.

The four panels of Fig. 3.2 show how the key properties of the bar change over time in both Au17 and TNG17. Panels a, b and c show the bar strength, pattern speed and ratio of $\mathcal{R}$ respectively. Panel d shows the evolution of the corotation radius and bar length for different snapshots. In panels b, c and d, data are shown only after the bar forms. All properties have been smoothed using a Savizky-Golay filter with a window length of 15 snipshots and a polynomial of order 3, this is to

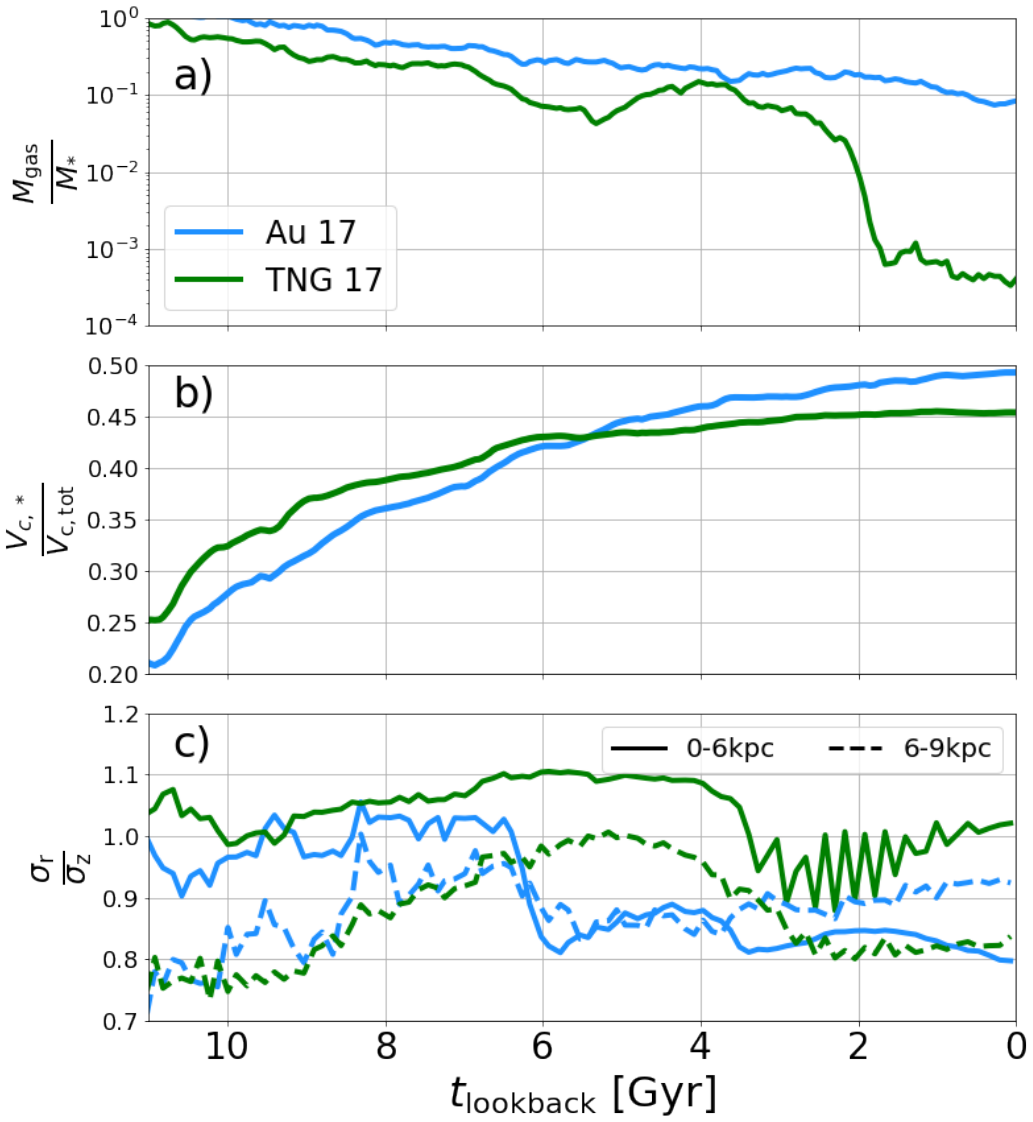

Figure 3.3: *a)*: The temporal evolution of the gas fraction measured inside 10kpc for Au17 (blue) and TNG17 (green). Note the log scale on the y-axis. *b)*: The evolution of the baryon dominance measured at 30kpc for Halo 17. *c)*: The ratio of radial to vertical velocity dispersion for Halo 17.

reduce any noise and provide greater clarity when viewing plots.

In the upper left panel of Fig. 3.2, $t_{\rm lookback}$ is plotted against $A_2^{\rm max}$. The bar formation time is slightly later in Au17 than TNG17, at 8.93 and 10.0Gyrs respectively. At high redshift, between 11 - 9Gyrs, the measured bar strength is somewhat noisy in both halos. At this time the disc is undergoing a lot of perturbations due to interactions and mergers and these affect the m = 2 Fourier mode.

At early times, after the bar formation, the bar is stronger in Au17 than TNG17.

After 6Gyrs the bar strength in Au17 drops and from then is consistently lower than TNG17. From 6Gyrs onward the bar strength in Au17 is fairly consistently, with occasional rises and falls. At the end of the simulation, TNG17 has a significantly stronger bar than Au17. Bar strength in TNG17 grows from when the bar forms until around 4Gyrs when it plateaus at a value of ~0.7. A summary plot of the temporal bar strength evolution for all the halos can be found in Appendix A.

The upper right panel, *b)*, shows how the pattern speed for each galaxy evolves over the course of the simulation. In Auriga 17, the fiducial case for comparison, starts with a lower pattern speed than TNG17. From 4Gyr onwards the pattern speed in TNG17 decreases steeply. On the other hand, while Au17 starts low, its pattern speed increases steadily, which indicates that the angular momentum of the bar and disc are increasing, it then plateaus around 4Gyrs.

Panel *c)* shows the evolution of $\mathcal{R}$ in both galaxies. The difference in how this parameter changes over the course of the simulation between the Auriga and TNG model is significant. In Au17 the value of $\mathcal{R}$ is consistently around 1. The evolution of TNG17 is only similar to Au17 at times before 7Gyrs, and from 9 - 4.5Gyrs remains within the bounds of the fast bar regime. From 5Gyrs onwards the $\mathcal{R}$ value of TNG17 increases until the end of the simulation, rising far above that of Au17. This occurs at the same time as the bar strength of TNG17 begins to increase and its pattern speed steeply declines. Such an increase in $\mathcal{R}$ indicates that the dominant mechanism of bar slowdown in TNG17 is dynamical friction. The evolution of $\mathcal{R}$ in Au17 suggests the opposite, that dynamical friction has little influence on the bar.

To examine the underlying cause of the development in $\mathcal{R}$ from panel *c)* I present the final plot of Fig. 3.2 in the lower right hand corner. Here the bar length is plotted against the corotation radius. Unlike the other three plots, lookback time is indicated by marker colours rather than on the x-axis. Plotting $R_{\rm bar}$ against $R_{\rm CR}$ allows an investigation into what is driving change in $\mathcal{R}$. The dashed lines on *d)* are at $\mathcal{R} = 1$, 1.4 and 2, as they are in panel *c)*. Outside of a few measurements made at $t_{\rm lookback} > 8$Gyrs, the circles (Au17) stay close to $\mathcal{R} = 1$. In Au17, over time the decrease in bar length is matched by a decrease in corotation radius, the latter caused by an increase in pattern speed. Comparing these results to TNG17 shows the evolution of both $R_{\rm bar}$ and $R_{\rm CR}$ to be quite different. Throughout the simulation, the bar length of TNG17 is shorter than that of Au17. For the final 5Gyrs of the simulation, the bar length changes by less than 0.5kpc. While at 8Gyrs $R_{\rm CR}$ in TNG17 is lower than Au17, over the course of the simulation it steadily increases, pushing the TNG17 bar out of the fast bar region. It is clear from this plot that the growth in corotation radius is driving the increase in $\mathcal{R}$ without

a relative increase in $R_{\rm bar}$. This is another indication that dynamical friction is playing a large part in the slowdown of the TNG bar.

3.1.2 Galaxy Properties

While examining the properties of the bar gives an idea of how the subgrid model affects the bar itself, these do not give the full picture of how the properties of the galaxy as a whole are changed by a different implementation of subgrid physics. To shed some light on global properties I present Fig. 3.3 which comes in three parts, all of which are plotted against $t_{\rm lookback}$.

The top panel shows the evolution of the gas fraction in the disc for Au17 and TNG17. I define this as the ratio of enclosed gas mass to enclosed stellar mass at a radius of 10kpc, with a restriction on the height of $|z| < 2$kpc. Note the logarithmic scale on the y-axis. The gas makeup of a galaxy is mostly affected by star formation, but gas accretion and winds that expel gas are also factors to consider. Overall it is expected that galaxies will have their gas fraction decrease as a function of time. In both Au17 and TNG17 this is true, they show a steady decrease in their gas content until 2Gyrs. At this time, while the gas fraction in Au17 continues to decrease in a steady fashion the same cannot be said for TNG17. At 2Gyrs the gas fraction of TNG17 decreases sharply, dropping an order of magnitude in the space of a few hundred Myrs. At the end of the simulation, the gas fraction in Au17 is more than two orders of magnitude greater than in TNG17.

The second panel of the figure shows the baryon dominance as a function of radius for both galaxies at 30kpc. This parameter is defined as the circular velocity of the stellar component as a proportion of the total circular velocity (as in Eq. 2.7). The rotation curve of a galaxy can be used to determine the enclosed mass of a component at a particular radius. As such, the baryon dominance can be thought of as a measure of the ratio of stellar to total enclosed mass. The middle panel in Fig. 3.3 shows how the baryon dominance within 30kpc evolves temporally in Halo 17 for both the Auriga and TNG subgrid models. Both grow over the course of the simulation from ~0.2 at 10Gyrs to ~0.5. The Auriga galaxy begins less baryon dominated than TNG but overtakes at 5Gyrs, from there the difference grows until $z = 0$. Baryon dominance has been linked to the amount of dynamical friction exerted on the bar by a massive halo (Debattista & Sellwood 2000), with increased baryon dominance leading to a faster bar, as measured by the $\mathcal{R}$ parameter. This is consistent with the results we find in this study, as Au17 has a greater baryon dominance than TNG17 and its bar is well within the fast bar regime at $z = 0$. In

contrast the bar in TNG17 is slow at the end of the simulation, at which point it has a lower baryon dominance.

The bottom plot of this figure describes the change in velocity dispersion over the course of the simulation, this being the standard deviation in the velocity of the stars, either in the vertical (z) or the radial ($\sqrt{x^2 + y^2}$) velocity component. Velocity values are a direct output of the simulation. Here I show the ratio between the radial and vertical velocity dispersion. If the radial dispersion grows, or the vertical dispersion decreases, the ratio would increase. The plot is split further into two different regions of radial distance, 0-6kpc (solid) and 6-9kpc (dashed). The former region is heavily influenced by the bar and contains information about what is happening in the central parts of the galaxy and the latter lies outside where the influence of the bar is strongest.

The velocity dispersion ratio in the 0 - 6kpc region tells an interesting story as the value for TNG17 is almost always greater, and in fact is always greater after 8Gyrs. A greater radial velocity dispersion is associated with a stronger bar, as bar supporting orbits are more radially elongated. The plot here shows that the radial dispersion is greater in TNG than Auriga relative to the vertical dispersion. In TNG17 the bar is also much stronger than in Au17 and remains so up to $z = 0$.

In both Au17 and TNG17, the ratio in the inner region takes a sharp drop at one point. For Au17 the drop is significant and occurs at 6Gyrs, in TNG17 it is less abrupt and takes place at 3Gyrs. This drop in the ratio is caused by an increase in the vertical velocity dispersion and is often associated with the buckling instability. Other characteristic signatures of the buckling instability are a reduction in bar length and the formation of a boxy-peanut bulge. The latter can clearly be seen in surface density plots of Au17 at 4Gyrs and at $z = 0$ but is absent at the bar formation time.

Outside the bar region, the trends velocity dispersion between 6 - 9kpc are less clear to decipher. Initially both models show an almost identical profile, with a rising velocity dispersion ratio until 6Gyr. After this time, TNG17 continues to rise where Au17. A similar decrease in the ratio occurs in TNG17 around 4Gyrs which reflects when the ratio decreases in the inner region at the same time. As this region is at a distance greater than the bar length, it gives a better picture of whether a disc is "hot" or "cold". From theoretical work (Athanassoula 2003), a hot disc should experience less bar slowdown than a slow one, due to a decreased angular momentum exchange with the halo. In the final 3Gyrs, Au17 has greater velocity dispersion in the 6 - 9kpc region than TNG17, at the same time $\mathcal{R}$ increases in TNG17 and does not in Au17.

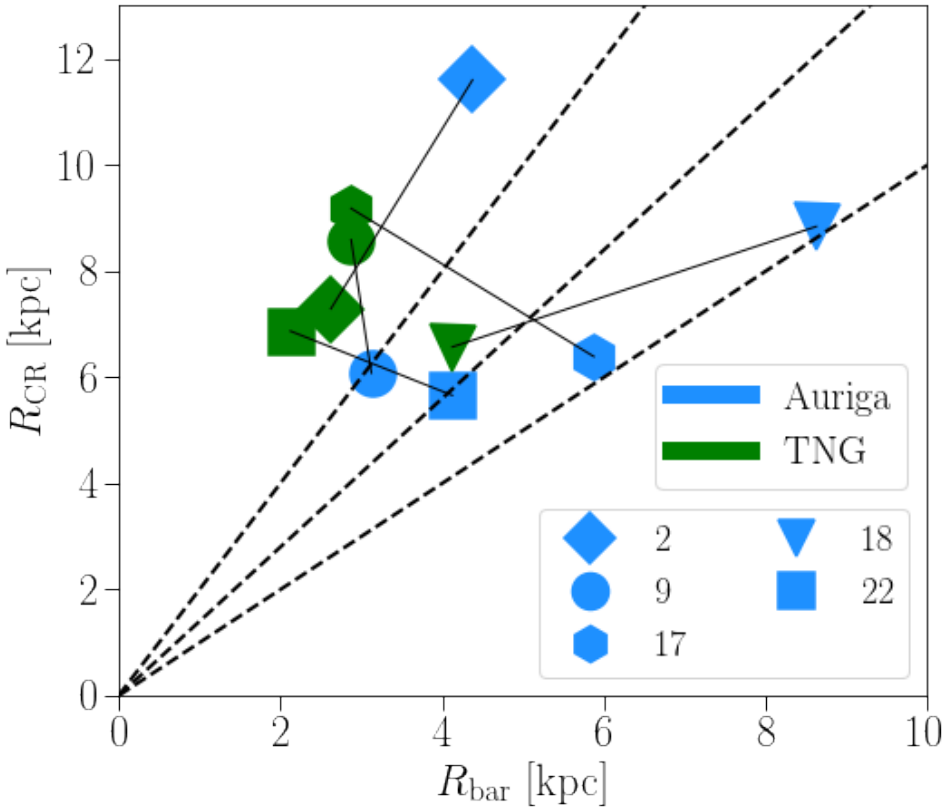

Figure 3.4: Bar length against corotation radius for all barred galaxies in our sample at $z = 0$. Each halo has a unique marker and the colour reflects the subgrid physics model. Halos of the same number are connected with a black line. Dashed lines show different values of $\mathcal{R}$ in the same way as Fig.3.2. Going anticlockwise from the right these lines are at $\mathcal{R} = 1$, 1.4 and 2.

3.2 Population Properties at z = 0

In this section I compare results for the population of halos at $z = 0$. The aim of this analysis is to compare two different subgrid physics models and to see how the properties of bars change when the baryonic physics changes. My focus therefore is comparing either a single halo run with both Auriga and TNG subgrid models (i.e. Au17 and TNG17), or to compare the sets of five halos with one another.

3.2.1 Bar Properties

Measuring $\mathcal{R}$ is the key to understanding the difference between the slowdown of bars in Auriga and TNG galaxies. In Fig. 3.4 the bar length is plotted against the

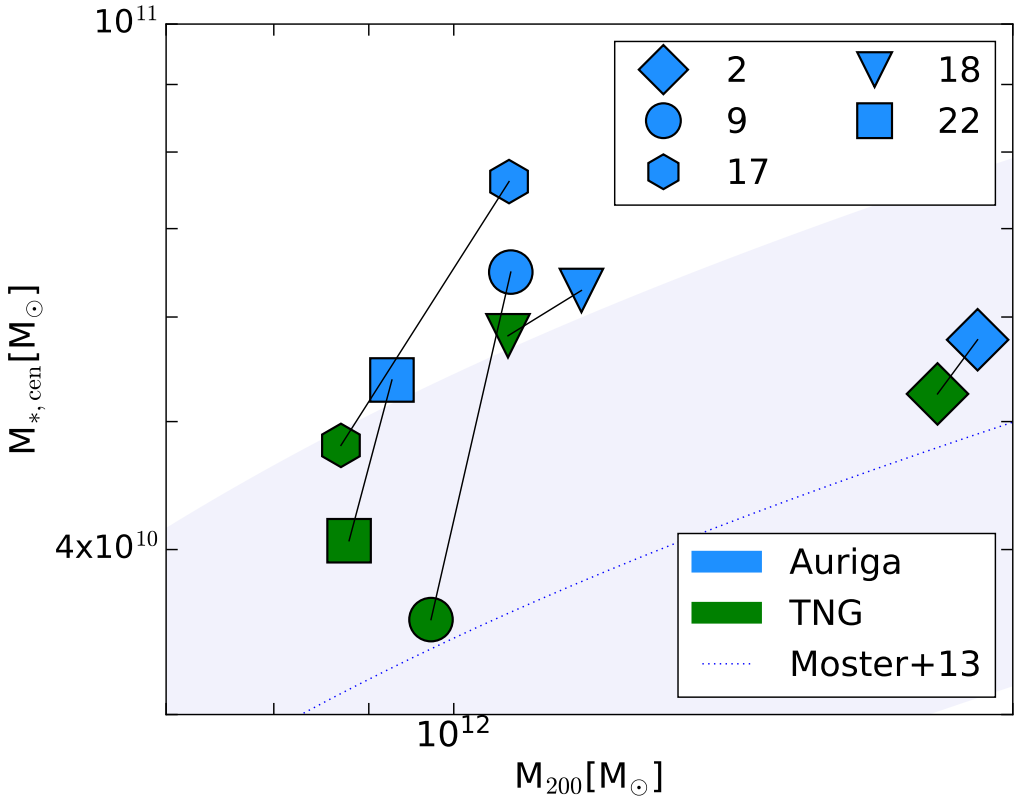

Figure 3.5: The virial mass of halos against their stellar disc mass, i.e. inside 30kpc and with |z| < 1kpc. The markers and colours match Fig. 2.2. Again solid lines are used to connect the Auriga halo with its TNG counterpart. The blue shaded area and dotted line represent the abundance matching relation derived in Moster et al. 2013.

corotation radius at $z = 0$. The value of $\mathcal{R}$ equal to the ratio of the axes. Travelling anti-clockwise around the plot $\mathcal{R}$ increases, indicating a slower bar. The dashed lines show fixed values of $\mathcal{R} = 1$, 1.4 and 2. The first two values are the boundaries of the fast bar regime. Each halo has two points on the plot with the same marker and a black line connecting the two. In this pair, the blue is the original Auriga galaxy and the green is the rerun with the TNG subgrid model. Auriga halos lie on the right hand side of the connecting lines, in other words, the bar length in Auriga is always greater than in TNG. This is supported further by the values given in Table 3.1. There is less of a trend when comparing the corotation radius in each halo, in three halos (9, 17 and 22) Auriga has a lower $R_{\rm CR}$. For the other two (2 and 18) the TNG galaxy has a shorter corotation radius. In most cases it is obvious from looking at the plot that of the two subgrid models Auriga has the lower value of $\mathcal{R}$ and therefore the faster bar. In the case of Halo 2 this is less clear but the data in Table 3.1 reveals that $\mathcal{R}$ is greater in the TNG galaxy for all halos.

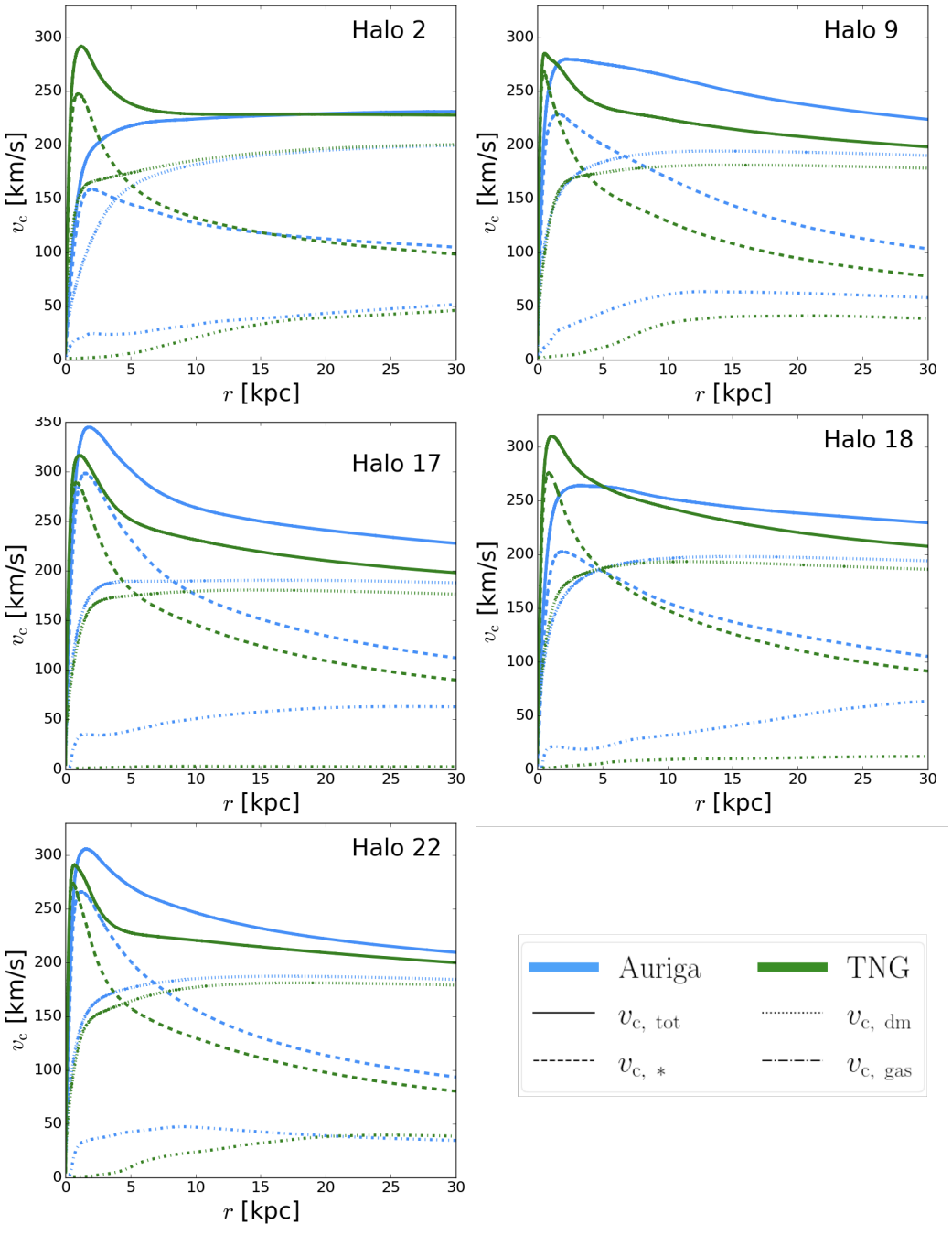

Figure 3.6: Rotation curves for each halo at $z = 0$. For each halo both subgrid models are present on the same plot, Auriga in blue and TNG in green. The circular velocity of the stellar (dashed), dark matter (dotted) and gaseous (dot-dash) components are also plotted.

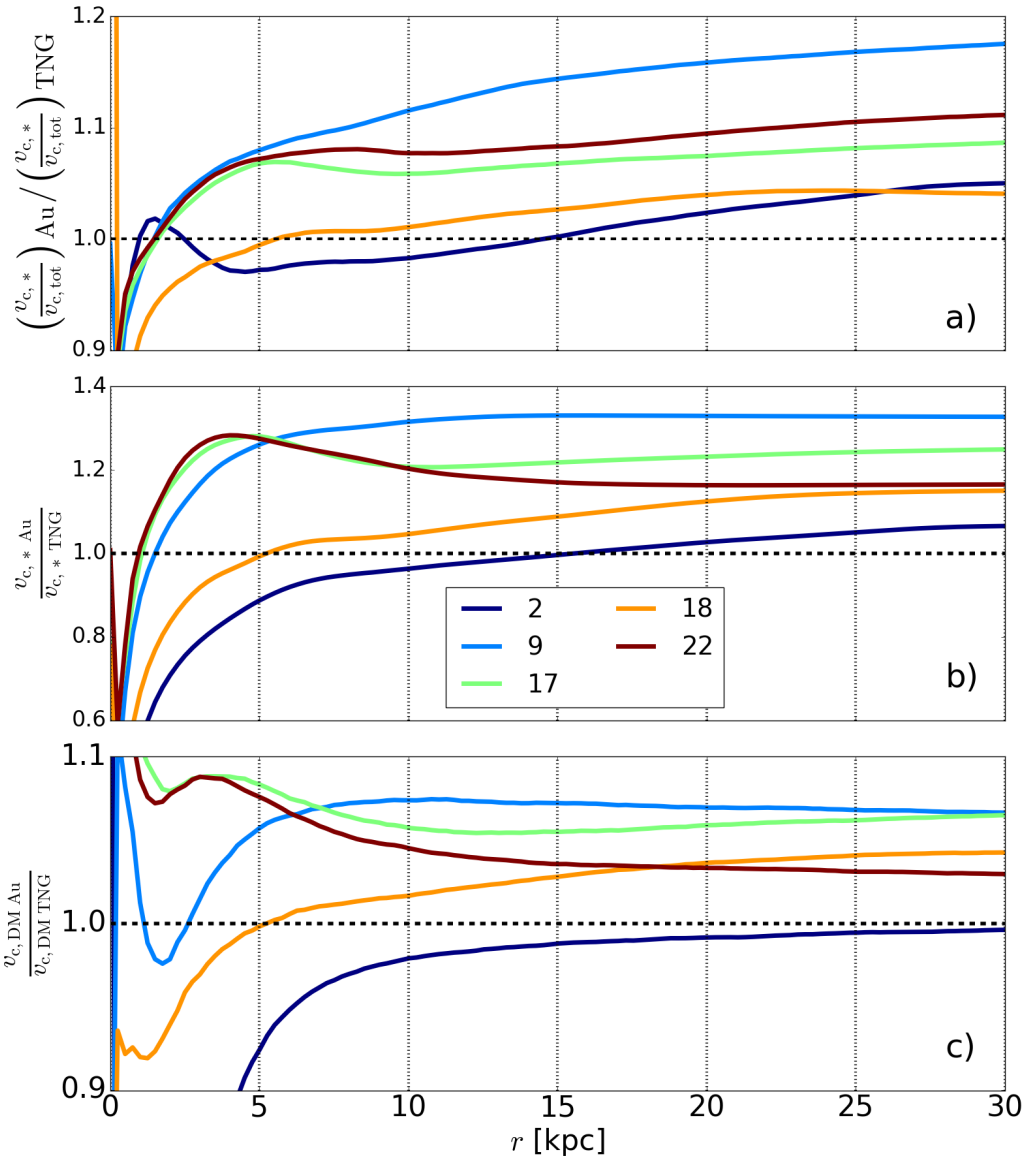

Figure 3.7: *a)*: The ratio of the baryon dominance between the two models as a function of radial distance from the centre of the galaxy at $z = 0$. A value greater than one (above the dashed line) shows that the halo is more baryon dominated at that radius for the Auriga model. *b)*: The ratio of the stellar component of v_c between the two models. *c)*: The same as *b)* but with the dark matter component. In both *b)* and *c)* the ratios are equivalent to the square root of the ratio of the enclosed mass of the stars and dark matter respectively.

Halo		A_2^{max}	R_{bar} kpc	Ω_p km/s/kpc	R_{CR} kpc	$\mathcal{R}$	$M_{*,cen}$ 10^{10} $M_\odot$	$\frac{M_{gas}}{M_*}$ $\times$ 100
2	Auriga	0.529	4.63	18.2	11.6	2.651	6.19	6.65
	TNG	0.598	2.38	31.7	7.29	2.777	5.48	2.42
9	Auriga	0.470	3.13	44.7	6.08	1.945	6.49	12.9
	TNG	0.772	2.88	26.4	8.59	2.988	3.54	6.91
17	Auriga	0.468	5.88	44.8	6.39	1.088	7.57	8.35
	TNG	0.707	2.88	25.4	9.18	3.193	4.80	0.04
18	Auriga	0.468	8.63	28.8	8.84	1.025	6.30	4.19
	TNG	0.521	4.13	38.8	6.57	1.593	5.81	0.17
22	Auriga	0.412	4.13	47.0	5.66	1.372	5.38	9.02
	TNG	0.741	2.13	32.6	6.87	3.233	4.06	3.37

Table 3.1: Properties of halos using different subgrid physics models at $z = 0$. Overall only five of the TNG reruns host bars at this time. For time evolution of A_2^{max} see Appendix A.

Three Auriga halos (17, 18 and 22) also have bars in the fast regime, $\mathcal{R} < 1.4$. This adds to recent work in which bars in ΛCDM simulations have stayed fast up to $z = 0$ (Fragkoudi et al. 2021), although we caution the reader that here we use a different method for deriving the bar length. Previous to this, the bar speed in galaxies from cosmological simulations had been shown to disagree with the speed of observed bars in the local universe, causing a tension between observation and theory (Algorry et al. 2017, Roshan et al. 2021).

While the subgrid physics models clearly produce bars with different $\mathcal{R}$, it is the global properties that are directly affected by the model itself. Looking at the overall characteristics of the halo population provides clues and insight into how they are affected by the subgrid model, from which they can be linked to the bar speed.

3.2.2 Galaxy Properties

The first galaxy property I examine is the stellar disc mass. In Fig. 3.5 the enclosed stellar mass within 30kpc ($M_{*,cen}$) is plotted against the virial mass of the halo (M_{200}) i.e. the enclosed mass at which the density of the halo is 200 times the critical density of the universe (ρ_{crit}). All halos within this sample are in the Milky Way analogue range of mass (1-2 $\times 10^{11}$). The original Auriga halos were selected to be in this halo mass range (Grand et al. 2017). Across the sample of galaxies the range of central stellar masses is quite small, within a factor of ~1.5. For a given halo the simulation run with Auriga subgrid physics always has a greater central stellar mass. There is a wide range of stellar mass differences, from Halo

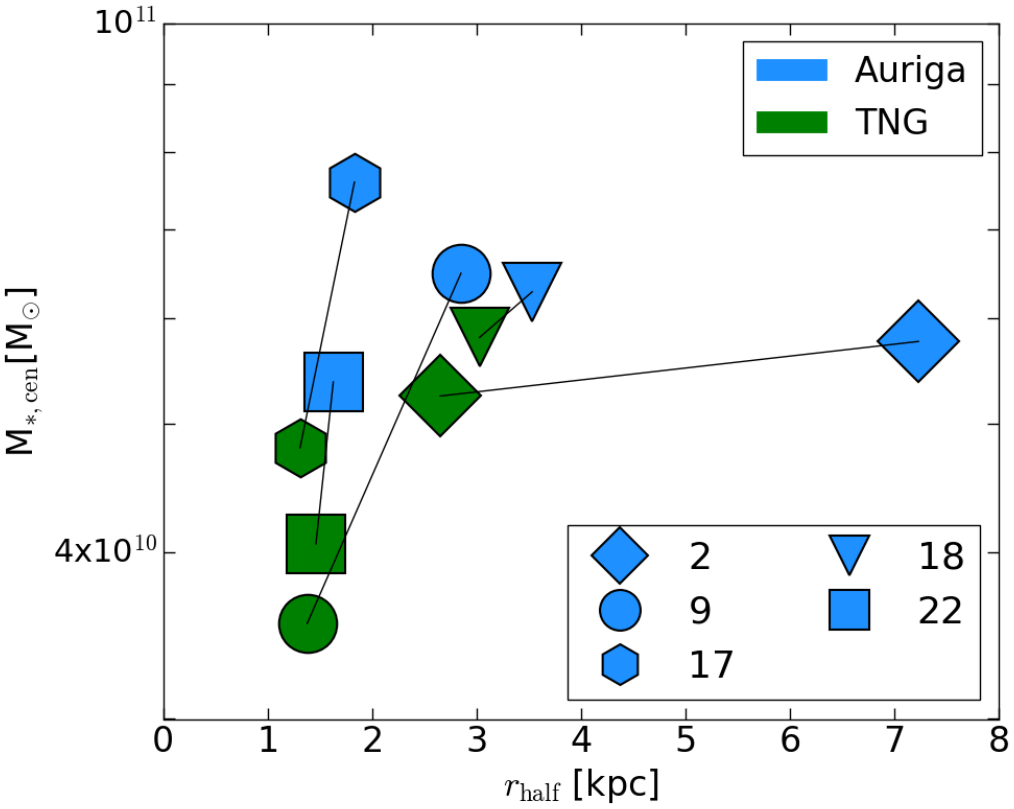

Figure 3.8: The central stellar disc mass (identical to Fig. 3.5) against the half mass radius of the same stellar population. A lower $r_{\rm half}$ value indicates that the disc is more concentrated towards the centre. Note the log scale on the y axis.

18 where the Auriga disc is only 8% more massive, to Halo 9 in which Auriga has 45% more mass. For this halo mass range, the Auriga subgrid physics model produces a more massive stellar disc than TNG. The blue dotted line and associated confidence interval is the abundance matching relation taken from Moster et al. 2013. Abundance matching is a way to match dark matter halos to galaxies, it is often used in large box cosmological simulations to calibrate star formation and feedback, so that simulated galaxies approximately follow this relation. It is added here to guide the eye about where the galaxies in the sample fall with respect to the relation. In Auriga, galaxies are above the relation as they form more stars for a given dark matter halo.

In order to probe the distribution of different components of the galaxies, I present Fig. 3.6. Here the circular velocity (Eq. 2.7) is plotted against the radial distance from the galactic centre, taken at $z = 0$. Across the rotation curves of the Auriga galaxies, there is quite a range of profiles for the overall rotation curve (solid line). For all the halos in the sample, and in both subgrid models, within approximately 5kpc the stellar component is dominating the shape of the total rotation curve.

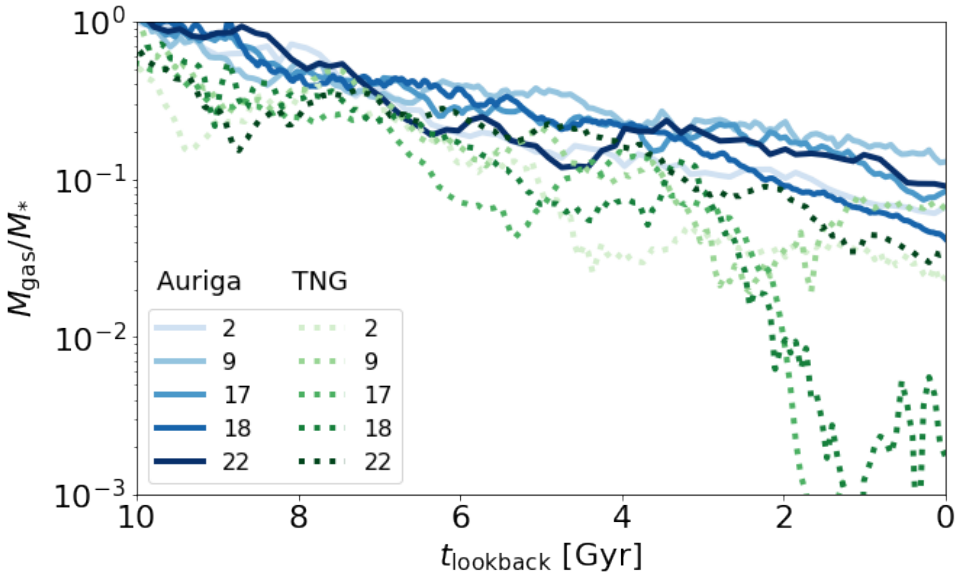

Figure 3.9: The gas fraction relative to the stars inside 10kpc over time of all Auriga and TNG galaxies. The lines follow a colour gradient according to halo number in blue for Auriga and green for TNG. Auriga galaxies have solid lines whereas the TNG are shown with dashed.

This gives insight into the central stellar mass of each galaxy. Those with a more peaked distribution have a greater concentration of their stellar mass within this region. In all halos, aside from Halo 17, the stellar component peaks at a greater value in the TNG model than Auriga. Outside of this region, the dark matter component dominates. In all the halos, v_c at 30kpc is greater in the Auriga model. The enclosed mass of the Auriga galaxies therefore must also be greater at this distance.

In all halos there is a greater circular velocity of gas in the Auriga model, and therefore a greater enclosed mass. The only deviation to this is in Halo 22 at radii greater than 20kpc, even then the difference between the two is marginal. In halos 2, 9 and 22 the profile of gas in TNG is similar, with a low $v_{c,\,gas}$ from 0 - 5kpc that rises afterward, suggesting that there is a low density of gas in the centre of these galaxies. This is to be expected as most star formation happens in this region, using up available gas by $z = 0$. In contrast, TNG17 and 18 have low $v_{c,\,gas}$ at all radii. The effect of gas on bars is still unclear, further discussion of which can be found in Chapter 4.

To quantitatively compare the rotation curves and mass distribution of the two subgrid models, I present Fig. 3.7. A figure in three parts, each a ratio between the two subgrid models of a different parameter. In all three plots a value above

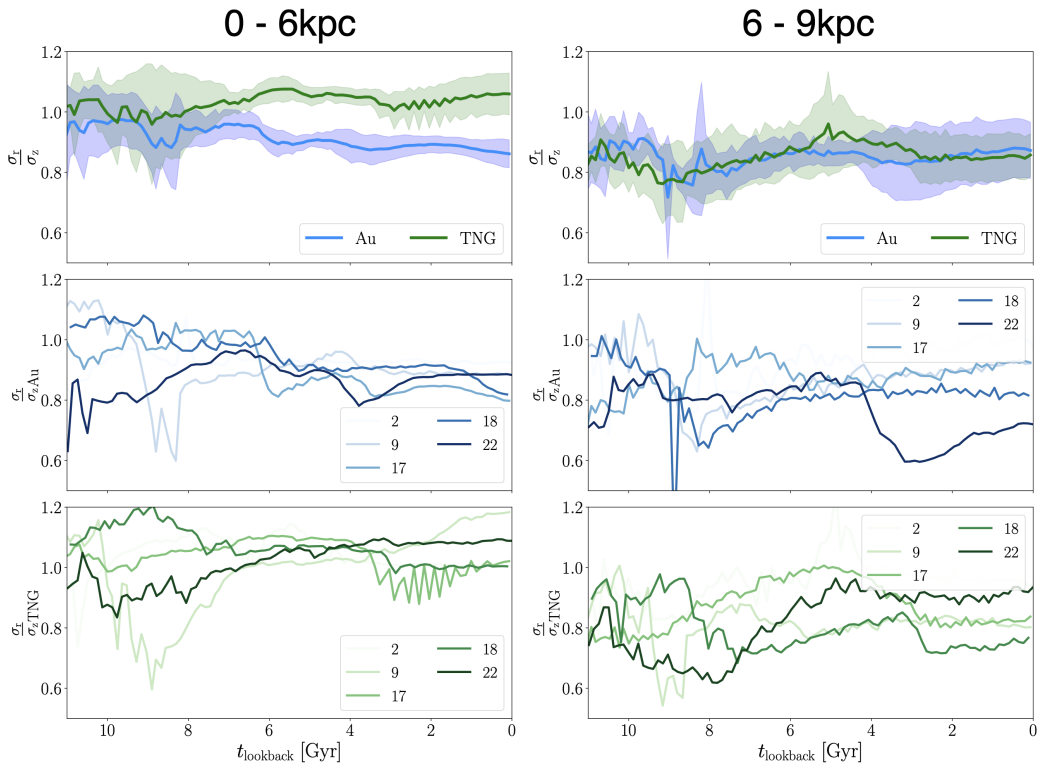

Figure 3.10: *a)*: The mean average of the ratio of the radial and vertical velocity dispersion across all the halos in the Auriga and TNG models. The shaded areas are 1σ. *b)* and *c)*: The ratio of the radial to vertical velocity dispersion over time for the individual halos in Auriga and TNG.

one indicates that the Auriga galaxy has a greater value than its TNG counterpart at the given radius. The dashed line on each panel is at a value of 1, where the value in each model is equal.

In the top panel, *a)*, the ratio of the baryon dominance between the Auriga and TNG models is plotted against radius. Baryon dominance is defined as the ratio of $v_{\rm c,\,*}$, the stellar component of the circular velocity, to $v_{\rm c,\,tot}$, the total circular velocity. This parameter was first linked to the slowdown of bars by Debattista & Sellwood 2000, who found that greater baryon dominance is associated with less interaction between the disc and halo, leading to less dynamical friction. In halos 9, 17 and 22, the baryon dominance is Auriga is greater than that in TNG at all distances outside of the central 2kpc. This is also true for Halo 18 after 5kpc. Halo 2 has a slightly different shape, peaking just above the dashed line at 2kpc before decreasing below 1 until 15kpc where the ratio then has a value greater than 1 until 30kpc. At 30kpc, all Auriga galaxies are more baryon dominated than TNG, ranging from a difference of 5% in Halo 18 to 20% in Halo 9. However, we find that the TNG galaxies are more baryon dominated in the central most regions, within

at least the inner ~2kpc. As we'll discuss below and as demonstrated in Fig 3.8, this is due to a higher central concentration of the TNG galaxies, even though they have lower stellar mass within 30kpc.

The middle panel, *b)*, shows the ratio of $v_{\mathrm{c},\,*}$ between the two subgrid models for all halos. This is equivalent to the ratio of square root of the enclosed stellar mass at a given radius. As was the case in Fig. 3.5, all Auriga halos have a greater mass of stars within 30kpc, as all the lines here are above 1 on the far right of the plot. In fact, for distances greater than 5kpc, all but one of the Auriga galaxies has a greater enclosed mass of stars. The exception again is Halo 2, in which the TNG model produces a greater stellar enclosed mass out to 15kpc. However, in both panels a and b we find that the TNG galaxies are more baryon dominated in the most central region.

A similar ratio can be found in the final panel, *c)*. In this case the ratio of $v_{\mathrm{c,\,dm}}$, the circular velocity of the dark matter, between the two subgrid models that is plotted. It is clear from the plot that $v_{\mathrm{c,\,dm}}$ is greater in the Auriga model than TNG at radii greater than 5kpc. The notable exception in this case is Halo 2, in which the ratio stays below 1 all the way out to 30kpc. While the Auriga halos have a greater mass of dark matter within 30kpc, the difference between the two is less than that for the stellar component, note the smaller range on the y-axis. The greatest difference in $v_{\mathrm{c},\,*}$ is in Halo 9 where the Auriga model has a value 33% more than TNG. In contrast, the largest difference in $v_{\mathrm{c,\,dm}}$ is in Halo 17 in which the Auriga value is only 5% greater than it is is in TNG.

From the three plots in this figure, I can draw the conclusions that the galaxies produced in the Auriga subgrid model have discs that are more dominated by stars than the TNG galaxies, within the inner 30kpc of the galaxy. On the other hand the mass of stars in the central 2-3kpc is greater in TNG than Auriga. Furthermore, we see that the dark matter halos of the Auriga galaxies also suffer larger adiabatic contraction due to the higher baryon content in the inner regions of these halos. Ultimately, while both the stellar mass and dark matter mass within 30kpc are higher in Auriga than in the TNG runs, the stellar mass increase is largest, which leads to more baryon dominated discs in the Auriga runs, as compared to the TNG runs.

The concentration of stellar discs is further revealed by Fig. 3.8. Here stars within 30kpc of the centre are chosen and their mass plotted against the half mass radius of the galaxy. A lower value of r_{half} indicates that the disc is more concentrated, as half the mass of stars is within a smaller distance of the centre. As in Fig. 3.5, a given halo is connected by a solid black line and the two subgrid models share a marker style. It is the case for every galaxy that the TNG subgrid model produces

a more concentrated disc, the difference in $r_{\rm half}$ shows a wide range, in Halo 22 the two models differ by only 0.17kpc. The other extreme is Halo 2, where $r_{\rm half}$ in TNG is half of its value in Auriga (2.65 and 7.23kpc respectively).

A summary of gas fraction across the sample, the proportion of gas mass to total mass in the disc, is given in Fig. 3.9. The plot shows how this property evolves for the Auriga and TNG halos over time, similarly to Fig. 3.3. Gas fraction in Auriga halos is always greater than the equivalent TNG halo across time. Across the galaxy population there is a steady decrease for most of the simulation time. The most conspicuous results are those of Halos 17 and 18 after 2Gyrs of lookback time. When examining Table 3.1 it is interesting to note that halos that have the greatest difference in their gas fraction (e.g. halos 17 and 18) also have the largest contrast their values of $\mathcal{R}$ at $z = 0$.

Velocity dispersion in the halo and the disc has been linked to bar slowdown through theoretical work (Athanassoula 2003) and is therefore another important property to analyse in this sample of simulations. Fig. 3.10 shows how the velocity dispersion of the stars in the disc changes over the course of the simulations for each galaxy. In each the ratio of radial ($\sigma_{\rm r}$) to vertical ($\sigma_{\rm z}$) velocity dispersion is plotted. The bottom two panels show in each figure show how this value changes for each galaxy individually over time. The top panels take the mean average of each model and plot this with a single standard deviation shaded above and below. On the left is the velocity dispersion ratio of stars within 6kpc, and on the right are the stars at a distance between 6 - 9kpc.

Many of the stars included in the left plot are part of the bar, therefore the value of $\frac{\sigma_{\rm r}}{\sigma_{\rm z}}$ is linked to the strength of the bar. Stars in bar supporting orbits will have a higher $\sigma_{\rm r}$, and as a result, a greater value of the ratio should correlate to a stronger bar. From Table 3.1, all of the TNG galaxies have bars that are stronger than Auriga at $z = 0$. Throughout the simulation, the mean average ratio of velocity dispersion is higher in the set of TNG galaxies. Over the course of the simulations the value of the ratio in both Auriga and TNG galaxies is consistent. Before ~6Gyrs, the galaxies may be going through mergers, or their bars have only recently formed, which is why the standard deviation at this time is much greater than afterward.

The right hand panel shows the evolution of the velocity dispersion ratio between 6 - 9kpc as a function of time. At this distance the bar has much less influence over the velocity dispersion and as such we can get a better idea of how "hot" or "cold" (as defined by the ratio of $\sigma_{\rm r}$ to $\sigma_{\rm z}$) the disc of a galaxy is, the greater the value of the ratio, the hotter the disc is. Athanassoula (2003) finds that if the disc is hotter its ability to exchange angular momentum with the halo component is diminished.

The effect of this is that bars experience less slowdown in hot compared to cold discs. The plot shows that in Auriga and TNG the evolution of the mean average velocity dispersion ratio is almost identical. The standard deviation, however, is much greater in this sample of stars than the stars in the inner disc. Overall, the velocity dispersion ratio for stars 6 - 9kpc from the centre of the galaxy is not significantly affected by the change in subgrid model.

Chapter 4

Discussion

To better understand the results presented in the previous section, it is important to place them within the context of the wider study of bar dynamics in cosmological simulations. In this work I have analysed a selection of galaxies from the Auriga suite of simulations. Alongside these I reran each while keeping all aspects of the simulation the same, aside from the subgrid model, which was changed to the one used in the IllustrisTNG simulations. Of the simulations I reran with TNG physics, five host a bar at $z = 0$ and as such make a useful comparison to the Auriga halos. The $\mathcal{R}$ parameter is the key indicator of whether a bar has been slowed down through dynamical friction with the dark matter halo. Analysing other key galaxy properties provides insight into what might be a causing a bar to be fast or slow. Subgrid physics models in cosmological simulations are largely responsible for aspects such as the amount of stars, as well as the distribution and kinematics of the stellar component of a galaxy. For instance, the ratio of the bulge to disc can be affected by the choice of subgrid model (e.g. Bonoli et al. 2016, Irodotou et al. 2022, etc.) and this in turn will also set the velocity dispersion of the disc (Grand et al. 2016).

In this section I will show how my results fit with those from other studies performed on observations, isolated halo simulations, and cosmological simulations. This will place my work into the wider context and add additional layers to the literature devoted to understanding the tension between bar speed in observed galaxies and those produced by cosmological simulations.

When making comparisons between bars in different galaxies, I am mostly interested in their $\mathcal{R}$ value. At the time a bar forms, we expect its length do be close to the corotation radius, and $\mathcal{R}$ close to 1 as a result. Over time, the bar will slow down and lose angular momentum via two mechanisms: lengthening of the bar supporting orbits, or interaction with the dark matter halo through dynamical

friction. In the first, bars redistribute angular momentum through the trapping of more stars from the disc into bar supporting orbits. During this process the bar length increases at the same time as the corotation radius, and $\mathcal{R}$ stays close to 1. In the latter, the bar experiences a torque from the dark matter halo via dynamical friction (Tremaine & Weinberg 1984b). In this case the corotation radius will increase without the relative growth of the bar length. This in turn causes the value of $\mathcal{R}$ to increase. While both processes can occur simultaneously, one mechanism will dominate over the other. If dynamical friction is driving the angular momentum exchange, $\mathcal{R}$ increases and at $z = 0$ the bar will be in the 'slow' regime, $\mathcal{R} > 1.4$ (Debattista & Sellwood 1998). If the dominant effect is the trapping of more stars into bar-supporting orbits, the corotation radius will stay close to the bar length, and $\mathcal{R}$ stays close to 1.

In Fig. 3.4, I find that bars in all five of the Auriga galaxies are faster than the equivalent galaxy that has TNG physics, the value of $\mathcal{R}$ when using the TNG model is always higher than in the equivalent Auriga halo. In all halos, the bar is longer in the Auriga case than it is in TNG. However, as can be seen by exploring halo 17 in detail, at high redshifts, the corotation radius of TNG17 is similar to its bar length, but then the corotation radius increases, while the bar length stays the same. This suggests that there is more dynamical friction in galaxies that use the TNG model as opposed to Auriga.

In Roshan et al. (2021) they compare observational data from Cuomo et al. (2020) with galaxies produced in the original TNG simulations. They find that TNG galaxies are much slower in comparison to the observed galaxies, with most of the simulated galaxies lying outside of the fast bar regime. Both those results and my own show that dynamical friction is the dominant slowdown mechanism in barred galaxies that have been produced using the TNG subgrid physics model. To be able to compare simulation data to observed, they use the same method of measuring bar length and pattern speed in both cases. Statistical work in this study shows that the $\mathcal{R}$ value they measure for the TNG simulations is incompatible with observations with a confidence greater than 12σ.

One study that measures the speed of the original Auriga galaxies is Fragkoudi et al. (2021). Here they find the $\mathcal{R}$ value for barred galaxies from the Auriga suite at $z = 0$. Three of the halos used in this study are the same as I use here: Au9, Au17 and Au18. The results of this paper are in agreement with my own, finding that Auriga galaxies tend to be in the fast bar regime. Both sets of results show that fast bars can exist in cosmological simulations that use ΛCDM cosmology.

My results are also in agreement with those found in Frankel et al. (2022), who used a sample of galaxies from the TNG50 simulations and observational data from

the survey. They take care throughout to adopt similar techniques when making measurements of simulated and observed galaxies; doing this ensures that they can make an apples to apples comparison. They show that the $\mathcal{R}$ value in the simulated galaxies is higher, the underlying cause of which is a short bar length rather than the bars being too slow. While they use different methods to make measurements of bar length and pattern speed to the ones I used here, their conclusions are based on a comparison between observed and simulated data sets. This makes it a useful analogue for my work as both their work and mine are based on comparing two sets of data. They find that their simulated bars are slow in comparison to observations, with a greater $\mathcal{R}$, but this slowness is not caused by a large corotation radius (which is linked to low pattern speed) but instead a bar that is too short.

In my own work I find that the TNG model produces galaxies with bars that are always shorter than the equivalent galaxy run with the Auriga model. At the same time, I see that in Auriga the value of $\mathcal{R}$ is lower at $z = 0$ than in the same halo in TNG. This suggests that during the evolution of the galaxies, dynamical friction from dark matter has a greater influence in TNG galaxies than it does in Auriga. As the bars in TNG are shorter at all times, for $\mathcal{R}$ to increase the corotation radius of TNG galaxies must grow more than Auriga over the course of the simulation. All of this poses the question, what causes the differences between the evolution of galaxies in Auriga and TNG?

Dark matter distribution has been linked to the value of $\mathcal{R}$ by a number of theoretical works (e.g. Debattista & Sellwood 1998, Athanassoula 2003 etc.). The influence of dynamical friction on bars has also been extensively studied (Tremaine & Weinberg 1984b). How dark matter is distributed throughout the central region of a halo, where the bar resides, will have a notable effect on the dynamical friction exerted on the bar and how much angular momentum is then exchanged with the halo. Theoretical work has also shown that a more halo dominated galaxy should have a stronger and slower bar due to the interaction between the halo and the disc (Athanassoula 2014).

From Fig. 3.7 it is clear that Auriga halos are more baryon dominated within 30kpc, with a difference between the two models ranging from 4% in Halo 18 to 17% in Halo 9. In central regions of the galaxy inside 5kpc, only three of the five halos are more baryon dominated in Auriga and all are more dominated in TNG within ~2kpc. At the same time, the bar length in Auriga is always longer than in TNG (see Table 3.1). If the elongation of bar supporting orbits is the dominant slow down mechanism the bar length grows more than if dynamical friction dominates. The combination of lower baryon dominance and a shorter bar length in galaxies using the TNG model suggests that dynamical friction is more dominant.

As the two sets of halos have exactly the same initial conditions and resolution, the difference in the subgrid model is the only factor that causes this difference. In Fig. 3.5 we have already seen that the Auriga galaxies have more stars within 30kpc at $z = 0$ than TNG, meaning that throughout the history of these galaxies there has been more star formation in this region. Feedback from AGN and SN can produce strong winds in the ISM. This affects the gas in two ways, the first is to heat it up, making it less likely to form stars and therefore contribute to the baryon dominance, the other is to expel gas from the galaxy altogether, leading to an insufficient amount of gas to continue to form stars. Fig. 3.9 and Table. 3.1 show that TNG galaxies have less gas at all times inside 30kpc. Studies have suggested that overly efficient feedback implementations could be behind galaxies that have a lack of baryons (e.g. Marasco et al. 2020), as we see in the TNG galaxies here.

Previous theoretical work has studied the effect of baryon dominance on the rotation speed of galactic bars, most notably Debattista & Sellwood (1998), and a lack of baryons is cited as a possible reason for slow bars in cosmological simulations in Fragkoudi et al. (2021). In this study they show that increasing the mass of the disc relative to the halo (in my work this is analogous to baryon dominance) decreases the value of $\mathcal{R}$ at $z = 0$. My work adds to this as the set of Auriga galaxies are more baryon dominated within 30kpc as well as hosting faster bars than their TNG counterparts.

For the purposes of my simulations, galaxies are made up of three constituent components, two of which have been addressed in the previous section. The third is gas, which contributes far less to the mass (see Fig. 3.3), especially at $z = 0$. There is still debate about how the bar and gas interact, with some studies suggesting it contributes to slowdown (Athanassoula 2003) and others that say the opposite (Athanassoula 2014). The results I present in Fig. 3.9 and the data in Table 3.1 suggest that gas is not retained to this level in either Auriga or TNG in the final Gyrs of the simulation. However, there is always a greater gas fraction in the Auriga disc compared to TNG at $z = 0$. In some, the difference is large, more than two orders of magnitude, and in the halos with the smallest difference, there is a factor of just less than 2 between them.

There are two mechanisms for the gas fraction to decrease, it can either be used to form stars or be expelled from the galaxy by winds produced by feedback (supernovae or AGN). As an explanation for the difference in gas makeup, if the former was the dominant cause of the lack of gas in TNG, there would be a greater mass of stars in the discs of those galaxies. From the previous section we know that this is not true. This leaves me to conclude that gas in TNG is expelled much

more efficiently through feedback than it is in Auriga. As the two models deal with feedback in different ways, this is one characteristic for which we can find a direct link between how the subgrid models differ and the resulting galaxy properties.

Theoretical work has suggested an anti-correlation between gas fraction and bar length (e.g. Berentzen et al. 2007 Villa-Vargas et al. 2010,Athanassoula 2014) meaning galaxies that are more gas rich should host shorter bars. I have found the opposite in my simulations, especially comparing between the two models. Auriga halos both have longer bars at $z = 0$ and have a higher gas fraction. However, recent observational work by Erwin (2019) conclude that the gas fraction in a galaxy at $z = 0$ has no significant relation to its bar length.

Another factor that has been analysed in theoretical work in relation to bar slowdown is the velocity dispersion of both the disc and the halo. In Athanassoula (2003), isolated halos with various initial values for the velocity dispersion are investigated. The conclusions of this work are that both a hotter disc and hotter halo can lead to a decreased rate of bar slowdown. It also finds that a stronger bar should lead to increased angular momentum exchange between the halo and the disc, with an increased bar slowdown rate as a result. When comparing these results to my own, we should be careful as Athanassoula (2003) uses the Toomre Q parameter, which includes σ_{r}, as their measure of velocity dispersion and not σ_{z}. In my own results I have presented the ratio of radial to vertical velocity dispersion. Where there is agreement between this study and my own work is that the stronger bars in TNG result in slower bars. For every halo at $z = 0$ the bar in Auriga has a lower bar strength and a lower $\mathcal{R}$ value.

Some studies have claimed the resolution of a simulation may be more dominant than subgrid physics in determining whether bars will be fast or slow (e.g. Frankel et al. 2022). In this work we keep the resolution fixed and use slightly different subgrid physics and as a result we find that these can have an important role. Our results reproduce the findings of Frankel et al. (2022), i.e. shorter bars in the TNG case, but with larger $\mathcal{R}$. This suggests that the difference found in Frankel et al. (2022) between $\mathcal{R}$ of TNG and observations (i.e. slow bars), which was not found in Auriga (Fragkoudi et al. 2021) could be due to the subgrid physics employed, rather than to differences in resolution.

Chapter 5

Conclusions

Over the course of this work I have explored the bar properties in cosmological simulations run with two different galaxy formation models. The goal of this work has been to study how the corotation radius over the bar length ($\mathcal{R}$), which is a measure of the slow down inflicted on bars by dynamical friction, is affected by subtle changes in the galaxy formation model, i.e. the subgrid physics. In particular, I wanted to explore how the subgrid physics affects the bar slowdown, and investigate in detail which physics properties in the galaxy are changed due to the subgrid physics, which would lead to differences in the $\mathcal{R}$ parameter. To do this, I selected a sample of galaxies from the Auriga cosmological simulation suite, and reran these same halos with the IllustrisTNG physics model, keeping the same initial conditions and resolution. For each halo, the properties of the simulation are the same apart for the subgrid physics model used. With this in mind, I can say that the cause of the differences between them is down to their subgrid physics alone. Here are the key results

- The choice of subgrid physics model does have an effect on the speed of bars. I have shown that when resolution, choice of cosmology, and initial conditions are held equal, a galaxy run with Auriga subgrid physics will produce a faster bar, with a lower $\mathcal{R}$, than the same halo run using the TNG model instead.
- Bars in Auriga and TNG start with a similar $\mathcal{R}$, but in the TNG galaxies $\mathcal{R}$ increases over time.
- At the end of the simulation, at $z = 0$, bars in TNG are shorter compared to Auriga bars, and have more concentrated discs.
- Stellar discs in Auriga have greater mass than their TNG counterparts. Halos run with TNG are less baryon dominated inside 30kpc and have a smaller

gas fraction at $z = 0$ when compared to the same disc in Auriga. These characteristics have been linked to bar slowdown by several previous works that study isolated halos. Alongside this, the stellar mass in the region $R < 30$kpc and $|z| < 2$kpc, is greater in Auriga galaxies than their TNG counterparts

- The velocity dispersion of the disc outside the bar region is the same in Auriga and TNG, which indicates that this does not play a major role in the slowdown of bars in TNG as compared to Auriga.

It is also worth noting that the only major difference between the subgrid models presented is in their treatment of the low accretion AGN feedback regime, this makes it clear that even this amount of difference between models can have a measurable impact.

5.1 Future Work

While the work I have presented here shows that the subgrid physics model has a definite impact on the speed of simulated bars, it leaves many open avenues for further inquiry. For instance, the two models I have compared are only a small sample of the many different models being used in cosmological simulations. Running these same halos in further subgrid models will only provide deeper insight into why bars are fast in some simulations and slow in others. Improvements and amendments to subgrid models are made constantly as new observational and theoretical work is carried out. Running these same halos again if either the Auriga or TNG models are updated would provide another set of data with which to compare the results presented here.

Another clear opportunity for analysis is to compare these halos with observational data. Until recently, the number of barred spirals in which the pattern speed could be measured was minimal and spread across different surveys, each with their own biases, which make for apples to oranges comparisons. The MaNGA survey (Bundy et al. 2015) has given access to data for close to 100 galaxies that the pattern speed can now be measured. If I were to apply the same method of measuring bar length and pattern speed to my simulation data, the two sets of galaxies could be compared without difficulty.

Resolution of simulations is another possible avenue for investigation. Performing the same analysis on these halos when run at different (either higher or lower) resolution would provide further insight into the interplay between how the subgrid model and resolution affect the dynamical properties of galaxies in simulation.

Of course, it is not only the bar speed that is affected by the change in subgrid physics model, now that the two sets of halos exist they could be used to compare how other aspects of the galaxies change when the different models are implemented. Two of the halos do not host a bar at $z = 0$ when rerun in TNG, the causes of which are just one avenue of investigation. There is no clear reason why a bar forms in some discs and not others, even with the wealth of barred spirals in big box cosmological simulations that have been produced in recent times. Even for a pair of halos that both form a bar in the simulations shown here, they do not usually appear at the same time. Further work could be done to see which aspects of the subgrid model are responsible for triggering bar formation (or lack thereof).

As cosmological simulations become more and more sophisticated, they will achieve ever greater accuracy when compared to the real universe. Subgrid physics models are key to unlocking this greater accuracy without imposing the monumental cost of simulating every star and cloud of gas individually. Here I have looked into one of the many galactic properties that are affected by changing how baryonic processes are modeled and reinforced the fact that barred spirals can stay fast up until $z = 0$ within the ΛCDM paradigm.

Bibliography

Aguerri, J. A. L., Mé ndez-Abreu, J., Falcón-Barroso, J., et al. 2015, Astronomy & Astrophysics, 576, A102

Algorry, D. G., Navarro, J. F., Abadi, M. G., et al. 2017, Monthly Notices of the Royal Astronomical Society, 469, 1054

Alonso, M. S., Coldwell, G., & Lambas, D. G. 2013, Astronomy & Astrophysics, 549, A141

Athanassoula, E. 1992, Monthly Notices of the Royal Astronomical Society, 259, 345

Athanassoula, E. 2002, The Astrophysical Journal, 569, L83

Athanassoula, E. 2003, Monthly Notices of the Royal Astronomical Society, 341, 1179

Athanassoula, E. 2005, Celestial Mechanics and Dynamical Astronomy, 91, 9

Athanassoula, E. 2014, Monthly Notices of the Royal Astronomical Society: Letters, 438, L81

Athanassoula, E. & Misiriotis, A. 2002, Monthly Notices of the Royal Astronomical Society, 330, 35

Beane, A., Hernquist, L., D'Onghia, E., et al. 2023, , 953, 173

Berentzen, I., Shlosman, I., Martinez-Valpuesta, I., & Heller, C. H. 2007, The Astrophysical Journal, 666, 189

Berman, R. H. & Mark, J. W. K. 1979, Astronomy & Astrophysics, 77, 31

Binney, J. & Tremaine, S. 2008, Galactic Dynamics: Second Edition

Blitz, L. & Spergel, D. N. 1991, The Astrophysical Journal, 379, 631

Bonoli, S., Mayer, L., Kazantzidis, S., et al. 2016, Monthly Notices of the Royal Astronomical Society, 459, 2603

Bundy, K., Bershady, M. A., Law, D. R., et al. 2015, The Astrophysical Journal, 798, 7

Chandrasekhar, S. 1943, The Astrophysical Journal, 97, 255

Cisternas, M., Sheth, K., Salvato, M., et al. 2015, The Astrophysical Journal, 802, 137

Contopoulos, G. 1980, Astronomy & Astrophysics, 81, 198

Contopoulos, G. & Grosbol, P. 1989, The Astronomy and Astrophysics Review, 1, 261

Corsini, E. M. 2011, Memorie della Societa Astronomica Italiana Supplementi, 18, 23

Corsini, E. M., Debattista, V. P., & Aguerri, J. A. L. 2003, The Astrophysical Journal, 599, L29

Cuomo, V., Aguerri, J. A. L., Corsini, E. M., & Debattista, V. P. 2020, Astronomy & Astrophysics, 641, A111

Cuomo, V., Lee, Y. H., Buttitta, C., et al. 2021, Astronomy & Astrophysics, 649, A30

Debattista, V. P. & Sellwood, J. A. 1998, The Astrophysical Journal, 493, L5

Debattista, V. P. & Sellwood, J. A. 2000, The Astrophysical Journal, 543, 704

Dehnen, W., Semczuk, M., & Schönrich, R. 2023, Monthly Notices of the Royal Astronomical Society, 518, 2712

Eckert, D., Gaspari, M., Gastaldello, F., Brun, A. M. C. L., & O'Sullivan, E. 2021, Universe, 7, 142

Ellison, S. L., Nair, P., Patton, D. R., et al. 2011, Monthly Notices of the Royal Astronomical Society, 416, 2182

Erwin, P. 2005, Monthly Notices of the Royal Astronomical Society, 364, 283

Erwin, P. 2019, Monthly Notices of the Royal Astronomical Society, 489, 3553

Erwin, P. & Sparke, L. S. 2002, The Astronomical Journal, 124, 65

Eskridge, P. B., Frogel, J. A., Pogge, R. W., et al. 2000, The Astronomical Journal, 119, 536

Faucher-Giguère, C.-A., Lidz, A., Zaldarriaga, M., & Hernquist, L. 2009, The Astrophysical Journal, 703, 1416

Fragkoudi, F., Grand, R. J. J., Pakmor, R., et al. 2020, Monthly Notices of the Royal Astronomical Society, 494, 5936

Fragkoudi, F., Grand, R. J. J., Pakmor, R., et al. 2021, Astronomy & Astrophysics, 650, L16

Frankel, N., Pillepich, A., Rix, H.-W., et al. 2022, The Astrophysical Journal, 940, 61

Gadotti, D. A. & Eustáquio de Souza, R. 2004, in The Interplay Among Black Holes, Stars and ISM in Galactic Nuclei, ed. T. Storchi-Bergmann, L. C. Ho, & H. R. Schmitt, Vol. 222, 423–426

Garma-Oehmichen, L., Hernández-Toledo, H., Aquino-Ortíz, E., et al. 2022, Monthly Notices of the Royal Astronomical Society, 517, 5660

Géron, T., Smethurst, R. J., Lintott, C., et al. 2021, Monthly Notices of the Royal Astronomical Society, 507, 4389

Ghosh, S. & Di Matteo, P. 2023, arXiv e-prints, arXiv:2308.10948

Goddy, J. S., Stark, D. V., Masters, K. L., et al. 2023, Monthly Notices of the Royal Astronomical Society, 520, 3895

Grand, R. J. J., Gó mez, F. A., Marinacci, F., et al. 2017, Monthly Notices of the Royal Astronomical Society, stx071

Grand, R. J. J., Springel, V., Gómez, F. A., et al. 2016, Monthly Notices of the Royal Astronomical Society, 459, 199

Guo, Y., Jogee, S., Finkelstein, S. L., et al. 2023, The Astrophysical Journal Letters, 945, L10

Heckman, T. M. 1980, Astronomy & Astrophysics, 88, 365

Hilmi, T., Minchev, I., Buck, T., et al. 2020, Monthly Notices of the Royal Astronomical Society, 497, 933

Hockney, R. W. & Hohl, F. 1969, , 74, 1102

Hohl, F. 1970, NASA Tech. Rep, 343

Huško, F., Lacey, C. G., Schaye, J., Nobels, F. S. J., & Schaller, M. 2024, Monthly Notices of the Royal Astronomical Society, 527, 5988

Irodotou, D., Fragkoudi, F., Pakmor, R., et al. 2022, Monthly Notices of the Royal Astronomical Society, 513, 3768

Khoperskov, S., Haywood, M., Di Matteo, P., Lehnert, M. D., & Combes, F. 2018, Astronomy & Astrophysics, 609, A60

Le Conte, Z. A., Gadotti, D. A., Ferreira, L., et al. 2023, arXiv e-prints, arXiv:2309.10038

Lee, G.-H., Woo, J.-H., Lee, M. G., et al. 2012, The Astrophysical Journal, 750, 141

Li, X., Shlosman, I., Heller, C., & Pfenniger, D. 2023, Monthly Notices of the Royal Astronomical Society, 526, 1972

Lynden-Bell, D. & Kalnajs, A. J. 1972, Monthly Notices of the Royal Astronomical Society, 157, 1

Marasco, A., Posti, L., Oman, K., et al. 2020, Astronomy & Astrophysics, 640, A70

Marinova, I. & Jogee, S. 2007, The Astrophysical Journal, 659, 1176

Masters, K. L., Nichol, R. C., Hoyle, B., et al. 2011, Monthly Notices of the Royal Astronomical Society, 411, 2026

Menendez-Delmestre, K., Sheth, K., Schinnerer, E., Jarrett, T. H., & Scoville, N. Z. 2007, The Astrophysical Journal, 657, 790

Miller, R. H. & Prendergast, K. H. 1968, The Astrophysical Journal, 151, 699

Moster, B. P., Naab, T., & White, S. D. M. 2013, Monthly Notices of the Royal Astronomical Society, 428, 3121

Nelson, D., Pillepich, A., Springel, V., et al. 2019, Monthly Notices of the Royal Astronomical Society, 490, 3234

Okamoto, T., Frenk, C. S., Jenkins, A., & Theuns, T. 2010, Monthly Notices of the Royal Astronomical Society, 406, 208

Ostriker, J. P. & Peebles, P. J. E. 1973, The Astrophysical Journal, 186, 467

Peschken, N. & Łokas, E. L. 2019, Monthly Notices of the Royal Astronomical Society, 483, 2721

Peters, W. L., I. 1975, The Astrophysical Journal, 195, 617

Petersen, M. S., Weinberg, M. D., & Katz, N. 2016, Monthly Notices of the Royal Astronomical Society, 463, 1952

Petersen, M. S., Weinberg, M. D., & Katz, N. 2023, arXiv e-prints, arXiv:2305.13366

Pillepich, A., Nelson, D., Springel, V., et al. 2019, Monthly Notices of the Royal Astronomical Society, 490, 3196

Pillepich, A., Springel, V., Nelson, D., et al. 2018, Monthly Notices of the Royal Astronomical Society, 473, 4077

Planck Collaboration, Ade, P. A. R., Aghanim, N., et al. 2014, Astronomy & Astrophysics, 571, A16

Roshan, M., Banik, I., Ghafourian, N., et al. 2021, Monthly Notices of the Royal Astronomical Society, 503, 2833

Roshan, M., Ghafourian, N., Kashfi, T., et al. 2021, Monthly Notices of the Royal Astronomical Society, 508, 926

Schaye, J., Crain, R. A., Bower, R. G., et al. 2015, Monthly Notices of the Royal Astronomical Society, 446, 521

Schiavi, R., Capuzzo-Dolcetta, R., Arca-Sedda, M., & Spera, M. 2020, Astronomy & Astrophysics, 642, A30

Schmidt, E. O., Mast, D., Gaspar, G., & Weidmann, W. 2023, Monthly Notices of the Royal Astronomical Society, 523, 1885

Sellwood, J. A. 2006, The Astrophysical Journal, 637, 567

Sellwood, J. A. 2014, Reviews of Modern Physics, 86, 1

Shlosman, I., Frank, J., & Begelman, M. C. 1989, Nature, 338, 45

Silva-Lima, L. A., Martins, L. P., Coelho, P. R. T., & Gadotti, D. A. 2022, Astronomy & Astrophysics, 661, A105

Springel, V. 2010, Monthly Notices of the Royal Astronomical Society, 401, 791

Springel, V. & Hernquist, L. 2003, Monthly Notices of the Royal Astronomical Society, 339, 289

Springel, V., White, S. D. M., Tormen, G., & Kauffmann, G. 2001, Monthly Notices of the Royal Astronomical Society, 328, 726

Toomre, A. 1964, , 139, 1217

Tremaine, S. & Weinberg, M. D. 1984a, The Astrophysical Journall, 282, L5

Tremaine, S. & Weinberg, M. D. 1984b, Monthly Notices of the Royal Astronomical Society, 209, 729

Valenzuela, O. & Klypin, A. 2003, Monthly Notices of the Royal Astronomical Society, 345, 406

Villa-Vargas, J., Shlosman, I., & Heller, C. 2010, The Astrophysical Journal, 719, 1470

Wegg, C., Gerhard, O., & Portail, M. 2015, Monthly Notices of the Royal Astronomical Society, 450, 4050

Weinberg, M. D. 1985, Monthly Notices of the Royal Astronomical Society, 213, 451

Weinberg, M. D. 1998, Monthly Notices of the Royal Astronomical Society, 297, 101

Weinberger, R., Springel, V., Hernquist, L., et al. 2017, Monthly Notices of the Royal Astronomical Society, 465, 3291

Williams, T. G., Schinnerer, E., Emsellem, E., et al. 2021, , 161, 185

Wu, Y.-T., Pfenniger, D., & Taam, R. E. 2018, The Astrophysical Journal, 860, 152

Yu, S.-Y., Kalinova, V., Colombo, D., et al. 2022, Astronomy & Astrophysics, 666, A175

Zee, W.-B. G., Paudel, S., Moon, J.-S., & Yoon, S.-J. 2023, The Astrophysical Journal, 949, 91

Appendix A

Bar Strength

Here is shown the bar strength as it evolves over time in all five halos for both the Auriga (top) and the TNG (bottom) subgrid physics models

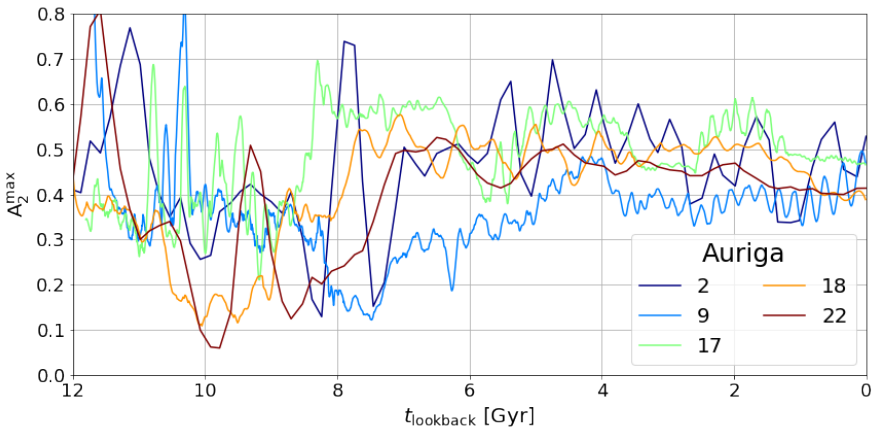

(a) $A_2^{\max}$ summary plot for Auriga

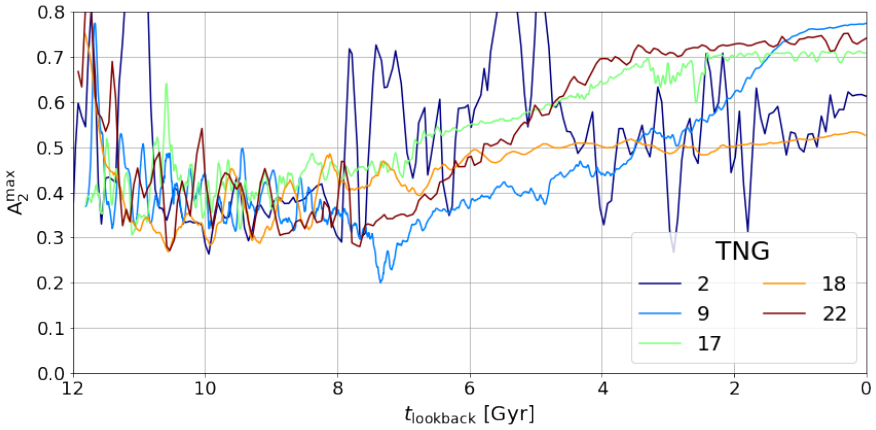

(b) $A_2^{\max}$ summary plot for TNG

Figure A.1

Colophon

This thesis is based on a template developed by Matthew Townson and Andrew Reeves. It was typeset with LaTeX 2_ε. It was created using the *memoir* package, maintained by Lars Madsen, with the *madsen* chapter style. The font used is Latin Modern, derived from fonts designed by Donald E. Kunith.